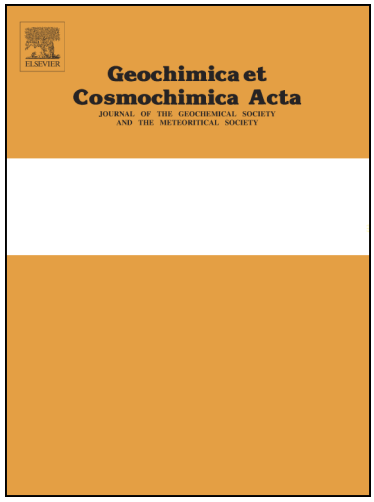

Elemental composition and optical properties reveal changes in dissolved organic matter along a permafrost thaw chronosequence in a subarctic peatland

Suzanne B. Hodgkins, Malak M. Tfaily, David C. Podgorski, Carmody K. McCalley, Scott R. Saleska, Patrick M. Crill, Virginia I. Rich, Jeffrey P. Chanton, William T. Cooper

PII: S0016-7037(16)30248-4
DOI: http://dx.doi.org/10.1016/j.gca.2016.05.015
Reference: GCA 9764

To appear in: *Geochimica et Cosmochimica Acta*

Received Date: 1 December 2015
Accepted Date: 7 May 2016

Please cite this article as: Hodgkins, S.B., Tfaily, M.M., Podgorski, D.C., McCalley, C.K., Saleska, S.R., Crill, P.M., Rich, V.I., Chanton, J.P., Cooper, W.T., Elemental composition and optical properties reveal changes in dissolved organic matter along a permafrost thaw chronosequence in a subarctic peatland, *Geochimica et Cosmochimica Acta* (2016), doi: http://dx.doi.org/10.1016/j.gca.2016.05.015

Elemental composition and optical properties reveal changes in dissolved organic matter along a permafrost thaw chronosequence in a subarctic peatland

Suzanne B. Hodgkins[a*], Malak M. Tfaily[b], David C. Podgorski[c], Carmody K. McCalley[d], Scott R. Saleska[e], Patrick M. Crill[f], Virginia I. Rich[g], Jeffrey P. Chanton[a], William T. Cooper[h]

[a] Department of Earth, Ocean, and Atmospheric Science, Florida State University, Tallahassee, FL, 32306
[b] Environmental Molecular Sciences Laboratory and Biological Sciences Division, Pacific Northwest National Laboratory, Richland, WA 99354
[c] National High Magnetic Field Laboratory, Florida State University, Tallahassee, FL, 32310
[d] Thomas H. Gosnell School of Life Sciences, Rochester Institute of Technology, Rochester, New York, 14623
[e] Department of Ecology and Evolutionary Biology, University of Arizona, Tucson, AZ, 85716
[f] Department of Geological Sciences, Stockholm University, 10691 Stockholm, Sweden
[g] Department of Microbiology, The Ohio State University, Columbus, OH, 43210
[h] Department of Chemistry and Biochemistry, Florida State University, Tallahassee, FL, 32306

* Corresponding author. Tel.: +1 850 320 5006; fax: +1 850 644 2581.
E-mail address: sbh10c@fsu.edu (S. B. Hodgkins).

Abstract

The fate of carbon stored in permafrost-zone peatlands represents a significant uncertainty in global climate modeling. Given that the breakdown of dissolved organic matter (DOM) is often a major pathway for decomposition in peatlands, knowledge of DOM reactivity under different permafrost regimes is critical for determining future climate feedbacks. To explore the effects of permafrost thaw and resultant plant succession on DOM reactivity, we used a combination of Fourier transform ion cyclotron resonance mass spectrometry (FT-ICR MS), UV/Vis absorbance, and excitation-emission matrix spectroscopy (EEMS) to examine the DOM elemental composition and optical properties of 27 pore water samples gathered from various sites along a permafrost thaw sequence in Stordalen Mire, a thawing subarctic peatland in northern Sweden. The presence of dense *Sphagnum* moss, a feature that is dominant in the intermediate thaw stages, appeared to be the main driver of variation in DOM elemental

composition and optical properties at Stordalen. Specifically, DOM from sites with *Sphagnum* had greater aromaticity, higher average molecular weights, and greater O/C, consistent with a higher abundance of phenolic compounds that likely inhibit decomposition. These compounds are released by *Sphagnum* and may accumulate due to inhibition of phenol oxidase activity by the acidic pH at these sites. In contrast, sites without *Sphagnum*, specifically fully-thawed rich fens, had more saturated, more reduced compounds, which were high in N and S. Optical properties at rich fens indicated the presence of microbially-derived DOM, consistent with the higher decomposition rates previously measured at these sites. These results indicate that *Sphagnum* acts as an inhibitor of rapid decomposition and CH_4 release in thawing subarctic peatlands, consistent with lower rates of CO_2 and CH_4 production previously observed at these sites. However, this inhibitory effect may disappear if *Sphagnum*-dominated bogs transition to more waterlogged rich fens that contain very little to no living *Sphagnum*. Release of this inhibition allows for higher levels of microbial activity and potentially greater CH_4 release, as has been observed in these fen sites.

1. INTRODUCTION

1.1. Decomposition in northern peatlands

Boreal and subarctic peatlands store between 270–455 Pg of carbon (Gorham, 1991; Turunen et al., 2002), of which ~277 Pg is in the permafrost zone (Schuur et al., 2008). This carbon has an uncertain fate as permafrost thaws due to continuing warming (Schuur et al., 2008). Although the Arctic is currently a net sink for carbon dioxide (CO_2), sequestering up to 0.8 Pg C/year mostly due to boreal forest growth, it is a net source of methane (CH_4) with annual emissions of 32–112 Tg CH_4/year, mostly from wetlands and lakes (Walter et al., 2007; McGuire et al., 2009; Thornton et al., 2015). Since CH_4 results in 25–33 times the radiative forcing of CO_2 (per kg of gas) on a 100-year timescale (Forster et al., 2007; Shindell et al., 2009), the response of CH_4 production to warming and permafrost thaw represents a major potential climate

feedback. Net CH_4 and CO_2 balances in thawing permafrost peatlands depend on plant production, which determines net autotrophic CO_2 uptake, and belowground decomposition, which determines heterotrophic CH_4 and CO_2 release. Belowground decomposition rates and pathways depend on inputs and reactivity of fresh plant litter and thawed permafrost carbon, soil water saturation (which controls belowground oxygen availability and aboveground plant species), and microbial metabolic pathways. The responses of these factors, and thus CH_4 and CO_2 emissions, to a warming climate remain uncertain. In this study, we focus on the effects of permafrost thaw and associated vegetation change on peatland organic matter chemistry.

1.2. Controls on DOM composition and lability

Anaerobic decomposition in peatlands is typically fueled by dissolved organic matter (DOM) rather than solid peat (Chanton et al., 2008). According to the size-reactivity model (Alperin et al., 1994; Amon and Benner, 1996; Burdige and Gardner, 1998), the first step in DOM decomposition is the degradation of high molecular weight macromolecules (HMW-DOM), defined as either >1000 or >3000 Da, into either monomeric or polymeric low molecular weight DOM (mLMW-DOM or pLMW-DOM). mLMW-DOM is more labile and can be rapidly degraded into CO_2 or used in methanogenesis (Conrad, 1999), while pLMW-DOM is more refractory and often accumulates. The reactivity of peatland DOM is thus an important control on both overall decomposition rates and the proportion of carbon released as CH_4.

Inputs from aboveground plants and belowground thawing permafrost (Ward and Cory, 2015) determine the initial composition and lability (defined here as the potential for rapid decomposition) of raw DOM that enters peat pore water. The main compounds that plants introduce to the DOM pool—either via direct input or via release from solid-phase peat—include carbohydrates, proteins, lipids, lignin-derived compounds, tannins and other phenolics, and other miscellaneous compounds such as chlorophyll (Kögel-Knabner, 2002; Kalbitz et al., 2003b). Microbial activity can then change DOM composition by several processes including preferential mineralization of more labile DOM compounds, alteration of existing compounds, or

assimilation into microbial biomass. Compounds that are usually enriched as others are degraded include lignin, humic acids, other aromatics, lipids, and alkyls with double bonds (Harvey et al., 1995; Glatzel et al., 2003; Kalbitz et al., 2003a, 2003b; Lorenz et al., 2007). Lignin in particular can only be degraded aerobically (Kirk and Farrell, 1987), and thus should accumulate in anaerobic peatlands.

DOM structure can influence decomposition not only directly via its reactivity, but also indirectly via reactions of specific DOM molecules. For example, humic substances and quinones can act as electron acceptors in anaerobic respiration, which due to more favorable energy yields outcompetes methanogenesis (Lovley et al., 1996; Cervantes et al., 2000; Heitmann et al., 2007; Keller and Bridgham, 2007; Blodau and Deppe, 2012; Bridgham et al., 2013). Phenolic compounds can also inhibit hydrolase enzymes and thereby suppress decomposition (Freeman et al., 2001, 2004).

Compared to other plant groups, litter from *Sphagnum* mosses decomposes unusually slowly. This slow decomposition is caused both directly by *Sphagnum* litter's recalcitrance, and indirectly by the inhibitory activity of specific compounds that also slow the decomposition of organic matter from other sources (Verhoeven and Toth, 1995). The main component of *Sphagnum* that contributes to its tanning properties (i.e., preservation of animal tissues) is the polysaccharide sphagnan (Painter, 1991), which is unusual for its reactive carboxylic acid groups contained within uronic acid monomers. These acids can form complexes with proteins, including those found in *Sphagnum* litter, to form recalcitrant humic substances via abiotic Maillard reactions (Painter, 1983, 1991). Enzyme activity necessary for biodegradation is also suppressed, both by complexation of enzymes with sphagnan (Painter, 1991), and by enzyme-inhibiting phenolics such as tannin-like compounds and sphagnum acid (Verhoeven and Toth, 1995; van Breemen, 1995; Verhoeven and Liefveld, 1997; Freeman et al., 2004). Experiments and field observations indicate that humic substances from *Sphagnum* inhibit methanogenesis, not only by competition as terminal electron acceptors, but also by possible direct toxicity to methanogens (Cervantes et al., 2000; Ye et al., 2012; Bridgham et al., 2013). Other factors,

which may contribute to *Sphagnum* peat's direct recalcitrance, include acidic pH and low nutrient availability, the latter caused in part by nitrogen entrapment within microbial biomass (Damman, 1988) and within sphagnan-derived humic acids (Painter, 1991).

In addition to external inputs, microbial activity also contributes compounds to DOM, resulting in a feedback mechanism in which DOM molecular structure both affects, and is affected by, microbial activity (Glatzel et al., 2003; Hodgkins et al., 2014). Compounds that can be directly produced by microbes, either as biomass or via extracellular reactions, include carbohydrates, proteins, aminosugars, and lipids (Ogawa et al., 2001; Kögel-Knabner, 2002; Kalbitz et al., 2003b; Kindler et al., 2009; Miltner et al., 2009), as well as uncharacterized molecules of unknown structure (Ogawa et al., 2001; Marschner and Kalbitz, 2003). Although microbially-derived material is commonly more labile than plant-derived material, a portion of it is refractory (Ogawa et al., 2001; Gruber et al., 2006) and becomes increasingly resistant to further degradation as it is recycled through the microbial food web (Kindler et al., 2006, 2009; Miltner et al., 2009). For example, although carbohydrates and peptides are usually considered more labile (Marschner and Kalbitz, 2003), they can sometimes accumulate either in DOM or in the solid phase due to microbial synthesis of large volumes of these compounds (Kögel-Knabner, 2002; Kalbitz et al., 2003b; Miltner et al., 2009), for instance in exopolymeric substances used for protection and adhesion (Wingender et al., 1999).

1.3. Analytical approach

Fourier transform ion cyclotron resonance mass spectrometry (FT-ICR MS) is an extremely powerful, ultrahigh-resolution method for obtaining detailed information on DOM elemental composition, and can thus reveal important differences in chemical composition between DOM from different sources and give insights on decomposition processes. Due to the very specialized instrumentation required and lengthy analysis process, this method is typically appropriate for targeted characterization of a limited number of samples. To complement FT-ICR MS, the analysis of DOM optical properties, including both absorption and fluorescence,

allows for higher sample throughput and identifies many of the same overall characteristics—including molecular weight (MW), aromaticity, and microbial vs. terrestrial origins (Tfaily et al., 2013).

Identification of the exact chemical structures responsible for different DOM optical properties, and thus robustly interrelating optical and FT-ICR MS data, presents significant challenges. Parallel factor analysis (PARAFAC) can aid in this task by deconvoluting DOM fluorescence spectra into the individual fluorophores that contribute to a complete spectrum (Stedmon and Bro, 2008). However, the properties associated with each fluorophore identified in DOM have not yet been unequivocally assigned (Ishii and Boyer, 2012). Recently, identification of the DOM molecules associated with different PARAFAC components has been accomplished by statistical correlation with compounds found by FT-ICR MS (Stubbins et al., 2014; Kellerman et al., 2015). However, even these types of analyses do not necessarily indicate that the molecular formulas associated with each component are directly contributing to its fluorescence. Factors that may lead to indirect correlations between molecular formulas and PARAFAC components include solution matrix effects on fluorescence properties, bio- and photodegradation reactions of fluorescing compounds into non- or differently-fluorescing compounds, and common sources and sinks of multiple compounds that fluoresce differently (Sharpless and Blough, 2014; Stubbins et al., 2014). Nonetheless, some of these factors may prove advantageous as fluorescing DOM molecules can provide valuable information on non-fluorescing molecules with which they commonly covary (Stubbins et al., 2014). More studies are clearly needed to strengthen the methods for predicting bulk DOM elemental composition based on the optical properties of chromophoric DOM.

To help address this knowledge gap, while also improving our understanding of warming-related changes in peatland DOM, we performed a full comparison of FT-ICR MS and optical properties for 27 DOM samples gathered from across a permafrost thaw succession with different peatland vegetation types in Stordalen Mire, a thawing peatland complex in subarctic Sweden. Specifically, we obtained UV/Vis absorbance spectra, and measured fluorescence by

163 excitation-emission matrix spectroscopy (EEMS), to aid in the interpretation of pore water DOM
164 elemental composition data obtained by FT-ICR MS. Methods used to analyze fluorescence
165 spectra included common indices for inferring aromaticity and MW, as well as relative
166 fluorophore intensities based on a PARAFAC model developed by Tfaily et al. (2015). This
167 represents the largest intercomparison of FT-ICR MS and optical data from wetland samples yet
168 published, and focuses on DOM from anaerobic peatland pore water from across a permafrost
169 thaw chronosequence. This study will not only significantly improve our ability to interrelate
170 DOM optical properties with DOM elemental composition, it will also provide a higher-
171 resolution understanding of previously observed changes in organic matter lability resulting from
172 permafrost thaw.

173 ## 2. METHODS

174 ### 2.1. Study site

175 Stordalen Mire (68.35°N, 19.05°E) is a peat plateau in subarctic Sweden underlain by
176 discontinuous permafrost, which is thawing as the region warms due to global change. Sites with
177 intact permafrost (palsas) are dry and ombrotrophic with an aerobic active layer, and are
178 vegetated by a combination of lichens, *Eriophorum vaginatum*, and ericaceous and woody
179 plants. In areas where the permafrost is degraded, land subsidence leads to varying degrees of
180 water inundation. In this study, we focused on these inundated sites because the intact palsas are
181 dry and therefore contain little to no DOM. The inundated sites are categorized based on the
182 classification system used by Hodgkins et al. (2014), McCalley et al. (2014), and Mondav et al.
183 (2014), whose site classifications are based on those of Johansson et al. (2006). In approximate
184 order of increasing time since inundation, these habitat types are as follows:

185 - **Recently thawed and collapsed thermokarst sinkholes ("col. palsa")** surrounded
186 by palsa; these holes contain no permafrost, can have a water table either above or
187 below the peat surface, and may be vegetated by a combination of species depending

188 on water level. In the collapsed palsa site measured in this study (site PHS; Table 1),
189 the dominant plants are *E. vaginatum* and *Sphagnum* spp.
190 • **Thawing *Sphagnum*-dominated bogs** with a water table below the peat surface,
191 which is often perched above a deeper permafrost layer.
192 • **Poor fens** containing a combination of *Sphagnum* spp. and tall sedges (e.g.,
193 *Eriophorum angustifolium*), which typically either have no permafrost or nearly
194 thawed permafrost.
195 • **Rich fens** dominated by tall sedges, such as *E. angustifolium* and/or *Carex rostrata*,
196 and which have no permafrost.

197 In terms of greenhouse gas balance, intact palsas are a net CO_2 source to the atmosphere
198 and approximately CH_4 neutral due to their low plant productivity combined with relatively fast
199 decomposition in their aerobic active layers (Christensen et al., 2004; Bäckstrand et al., 2010;
200 McCalley et al., 2014). Little is known about the net carbon and greenhouse gas balances of
201 collapsed palsa sinkholes, but incubation experiments suggest that decomposition within
202 collapsed palsas releases very little CH_4 and CO_2 compared to the other sites (Hodgkins et al.,
203 2014). Bogs and fens are net CO_2 sinks due to their higher primary productivity, but their
204 anaerobic subsurface conditions make them sources of atmospheric CH_4 (Bäckstrand et al., 2010;
205 McCalley et al., 2014). In the case of fens, this CH_4 production is so high that their net radiative
206 forcing impact per unit area over a 100-year timescale is approximately 7 times that of intact
207 palsas and 28 times that of bogs (Bäckstrand et al., 2010). Due to fens' high CH_4 emissions and
208 the expansion of fens and other wet sites with permafrost thaw (Malmer et al., 2005; Johansson
209 et al., 2006; Bäckstrand et al., 2010), the net annual greenhouse gas balance of the entire mire (in
210 terms of radiative forcing) increased by ~21% between 1970 and 2000 (Bäckstrand et al., 2010).

211 **2.2. Sampling and pH measurements**

212 Twenty-seven pore water samples were gathered from the active layer of seven inundated
213 sites at Stordalen in varying stages of permafrost thaw and plant species composition, including a

collapsed palsa site (PHS), three different bog sites (Bog1, SOS, and S), a poor fen site with *E. angustifolium* growing in a bed of *Sphagnum* (EOS), and two fully-thawed rich fen sites dominated by *E. angustifolium* (E and Fen2) (Table 1). These samples were used to characterize the changes in DOM elemental composition and optical properties along the gradient of permafrost thaw.

Pore water was gathered by syringe suction through a 1-m long, 0.5-cm-diameter stainless steel tube with holes drilled along the bottom 3 cm, then filtered through 0.7-µm Whatman GF/F glass microfiber filters into 120-mL brown borosilicate bottles. The pH was measured on-site with an Oakton Waterproof pHTestr 10. The bottles were frozen within 8 h of collection and stored frozen until analysis.

2.3. DOC concentrations

Dissolved organic carbon (DOC) concentrations were measured by high-temperature catalytic oxidation on a Shimadzu Total Organic Carbon analyzer with a non-dispersive infrared detector. Each sample was analyzed with triplicate measurements, which always had a coefficient of variance of <2%.

2.4. FT-ICR MS

Although the samples were all freshwater, even small amounts of salts can affect FT-ICR MS ionization efficiencies. The samples were therefore desalted by solid phase extraction (SPE) with PPL cartridges (Dittmar et al., 2008). 30 mL of each sample (acidified to pH = 2 with HCl) was extracted, and the DOM was eluted in methanol (see Tfaily et al. (2012) for detailed methods). Based on an extraction efficiency of 62% for freshwater samples (Dittmar et al., 2008), the final DOC concentrations in the extracts ranged from 0.2–0.3 mg/mL for collapsed palsas; 0.1–0.4 mg/mL for bogs; 0.1–0.2 mg/mL for poor fens; and 0.02–0.1 mg/mL for rich fens.

The extracted samples were analyzed on a custom-built Fourier transform ion cyclotron resonance mass spectrometer (FT-ICR MS) with a 9.4 Tesla superconducting magnet at the

National High Magnetic Field Laboratory (NHMFL) (Tallahassee, FL). Negatively-charged molecular ions were generated with a home-built electrospray ionization (ESI) source. The samples were injected into the ESI source at 0.5 μL/min with a syringe pump connected to a 50-μm-internal-diameter fused silica tube. The experimental parameters were chosen based on previous fulvic acid characterizations for optimization of DOM MS methods (Stenson et al., 2003), and were as follows: needle voltage, −2.5 kV; tube lens, −340 V; and heated metal capillary, 8 W. The ion accumulation time per scan was adjusted to account for the differences in SPE extract concentrations, with longer accumulation times used for more dilute samples. This results in approximately the same number of ions reaching the ICR analyzer cell, regardless of sample concentration. Each spectrum was produced as a sum of 200 individual scans, and the average resolving power ($m/\Delta m_{50\%}$) at 451 Da was >700,000. Spectra were not blank-corrected because it is not possible to know the ionization efficiency of compounds that produce background signals in the presence of the overwhelming concentration of extracted DOM compounds. Our interpretations of mass spectra rely on observed differences in samples, and this "differencing" removes any contributions from background peaks.

2.5. UV/Vis absorption spectroscopy

The UV/Vis absorbance of each pore water sample was measured between 250 and 400 nm on a Cary Varian 100 dual beam UV/Vis spectrometer using a 10 mm Suprasil cuvette, with blank-correction using Milli-Q water in an identical cuvette measured alongside the sample. To prevent inner filter effects during absorbance measurements, samples with absorbances >0.8 at a wavelength of 350 nm or >2.2 at 254 nm (absorbance units; AU) were diluted with Milli-Q water until they had absorbances below these values. To prevent inner-filter effects during subsequent fluorescence measurements, samples were further diluted with Milli-Q water until they had an absorbance of ≤0.02 AU at 350 nm (Kowalczuk et al., 2003); after adjusting for dilution, the absorbance values of these highly diluted samples (≤0.02 AU at 350 nm) were within 5% of the absorbance values of the same samples measured at higher concentration (≤0.8 AU at 350 nm,

used in calculations with UV/Vis data). To make these measurements reflective of the *in situ* absorption and fluorescence of the samples, no pH adjustments were carried out. While we recognize that metals can influence absorption and fluorescence through quenching, metal concentrations in peatland pore water are in the ng/L range (Rausch et al., 2006), several orders of magnitude lower than the DOC concentrations in our samples (Table 1). Each sample was measured in duplicate.

2.6. Fluorescence (EEMS)

Fluorescence spectra (after samples were diluted to absorbance ≤0.02 AU at 350 nm) and a blank (Milli-Q water used for dilution) were measured in a 10-mm path length quartz cuvette using a Jobin Yvon SPEX Fluoromax-4 spectrometer with a Xenon lamp source. Excitation wavelengths were scanned from 240–500 nm in 5 nm increments, and emission was measured from 290–600 nm in 2 nm increments. Data were gathered in signal/reference mode, normalizing the fluorescence emission signal with the excitation intensity. The band pass for both excitation and emission monochromators was 5 nm, and the integration time was 0.1 s.

2.7. Calculations

2.7.1. Elemental composition

MIDAS Predator Analysis and Molecular Formula Calculator software from the NHMFL were used for internal calibration and molecular formula assignment, respectively. FT-ICR MS spectra were calibrated with two internal homologous series of formulas separated by 14 Da (representing $-CH_2$ groups), and the mass accuracy was calculated as <1 ppm for singly charged ions across the mass distribution (m/z = 170–800). Molecular formulas were calculated for signals >6σ RMS baseline noise (Tfaily et al., 2011; 2013) based on the presence of C, H, O, N, and S (Stenson et al., 2003), and only ion masses with a mass accuracy of ±1 ppm compared to the IUPAC exact mass were included in the data set. The abundance threshold of >6σ above the RMS baseline noise was chosen because it results in a less than 1% probability of picking peaks

attributed to random noise (this threshold is twice the 95% confidence detection limit of 3σ RMS noise that is generally accepted for analytical measurements), while maximizing the number of formulas that can be assigned (small peaks below this threshold contribute <1% to the overall sum of peak intensities). Spacing of 1.0034 Da between ^{13}C isotopologues of the same molecule ($^{12}C_n$ and $^{12}C_{n-1}{}^{13}C_1$) confirmed that all ions with assigned formulas were singly charged (Brown and Rice, 2000; Kujawinski et al., 2002). In each sample, the relative abundances of all assigned formulas were normalized to have a sum of 100, and the formulas containing ^{13}C were then removed. Reproducibility of assigned formulas in replicate samples was good (Sleighter et al., 2012): A pair of replicates from a bog (S.0.38a and S.0.38b) shared 86% of formulas in common while a pair of replicates from a rich fen (E.0.38a and E.0.38b) shared 87% of formulas, and there were no systematic differences in the elemental compositions of the remaining non-matching formulas in either pair of replicates. In contrast, pairs of unique (non-replicate) samples shared, on average, 64% of formulas in common (range 33–87%), and there were often systematic differences in elemental composition (see Results, "3.2. FT-ICR MS").

For initial analysis of differences between bogs and rich fens, data from six bog samples and six rich fen samples from similar sampling dates and depths (specifically, bog samples S.0.38a, S.0.38b, SOS.1.10, SOS.1.31, S.2.12, and S.2.70, and fen samples E.0.38a, E.0.38b, Fen2.1.15, Fen2.1.30, E.2.7, and E.2.70) were selected. The normalized relative abundances in each sample (normalized to a sum of 100, as described above) were then used to calculate average relative abundances for each formula across all 6 samples in each habitat type (bog and rich fen), using an abundance of 0 for formulas not observed in a given sample. The average abundance of each formula in rich fens was then subtracted from its average abundance in bogs, giving a measure of the formula's "more bog-like" (positive differences) or "more fen-like" (negative differences) prevalence. The formulas were then visualized as 3-D van Krevelen (Fig. 1a) and molecular size (Fig. 1b) plots, with formulas more abundant in bogs or fens indicated by color.

To compare changes in elemental composition across all 27 samples, abundance-weighted average MW, O/C, H/C, N/C, and S/C were computed for each sample. For example, the abundance-weighted average O/C of each sample was calculated as:

$$O/C_{total} = \frac{\sum_{i=1}^{p}(a_i \times nO_i)}{\sum_{i=1}^{p}(a_i \times nC_i)} \quad (1)$$

where O/C_{total} is the abundance-weighted average O/C, p is the number of assigned formulas in the sample, i is the summation index, a_i is the relative abundance of formula i, nO_i is the number of oxygen atoms in formula i, and nC_i is the number of carbon atoms in formula i. The other average elemental ratios were calculated in a similar manner. The abundance-weighted average MW in each sample was calculated as:

$$MW_{avg} = \sum_{i=1}^{p}(a_i \times MW_i) \quad (2)$$

The formulas were also categorized into classes according to their H/C and O/C (Kim et al., 2003; Sleighter and Hatcher, 2007; Hodgkins et al., 2014). These classes included lipid-like, protein-like, aminosugar and carbohydrate-like (AS.carb), unsaturated hydrocarbon (UH), condensed aromatic (CA), lignin-like, and tannin-like compounds (Table 2, Fig. 1a). It is important to note that due to the different ionization efficiencies of different compounds, the relative abundances of different compound classes do not directly correspond to actual concentrations, but should rather be interpreted as relative amounts for different samples. For example, although the apparent relative abundance of the AS.carb class in all samples is nearly zero due to the very low ionization efficiencies of carbohydrates, the actual fraction of aminosugars and carbohydrates in DOM is likely much higher.

2.7.2. Bulk optical properties

The UV/Vis absorbance spectra were averaged across duplicates, then multiplied by the dilution factor (undiluted/diluted concentration ratio) and divided by the path length of the cuvette to obtain absorbance per meter (m^{-1}) in the undiluted samples.

Each EEMS fluorescence spectrum was corrected for Raman scattering, Rayleigh scattering, and dilution using FL Toolbox 1.91 software in MATLAB according to the methods of Gonsior et al. (2008). Raman and Rayleigh scattering peaks were eliminated by removing portions (±10–15 nm FW) of the fluorescence signal centered on the respective scatter peaks (Zepp et al., 2004). As suggested by Lawaetz and Stedmon (2009), the data were then normalized to the Raman intensity of the blank (350ex/397em, 5 nm band pass; Tfaily et al., 2013) and converted to Raman-normalized quinine sulfate equivalents (QSE) in ppb through an external calibration (Coble et al., 1998). To correct the spectra for dilution, the scatter-corrected fluorescence of the blank was subtracted, and the resulting values were then multiplied by the dilution factor to obtain the fluorescence of the undiluted sample.

Based on the DOC concentrations, UV/Vis absorbance spectra, and EEMS spectra for each sample, we determined the following bulk optical properties that relate to molecular structure:

- Specific UV absorbance (SUVA), which is defined as the ratio of the absorbance at 254 nm (m^{-1}) to the DOC concentration (mg/L), and increases with aromaticity (Weishaar et al., 2003).
- Biological index (BIX), defined as the ratio of emission intensities at 380 nm to 430 nm at an excitation wavelength of 310 nm. In a study of estuarine samples, Huguet et al. (2009) found that BIX increases with the contribution of microbial exudates to the DOM pool, with values <0.6 indicating little microbial activity and values >1 indicating DOM of primarily microbial origin.
- Humification index (HIX), defined as H/L, where H and L are the integrated emission intensities from 434–480 nm and 300–344 nm (respectively) measured at an excitation wavelength of 255 nm (Zsolnay et al., 1999). Since this index is positively correlated with aromaticity, it often increases with decomposition as organic matter becomes more humified (Kalbitz et al., 2003b; Hur, 2011). However, the

accumulation of microbial exudates during decomposition can also lower HIX (Kalbitz et al., 2003b; Birdwell and Engel, 2010; Tfaily et al., 2015).

- Emission wavelength of maximum fluorescence of peak C as defined by Coble (1996) (Em_{max}), which increases with unsaturation, with longer wavelengths indicating more conjugated molecules and condensed aromatic structures (Senesi, 1990).
- Ratio of peak C intensity (QSE) (F_{max}) to the absorption coefficient at 340 nm (A_{340}, defined as the absorbance in m^{-1} times 2.303). This ratio, F_{max}/A_{340}, decreases with increasing MW (Stewart and Wetzel, 1981; Baker et al., 2008).

2.7.3. PARAFAC model

Due to the relatively small number of samples used in this study, and the consequently poor statistical reliability of a PARAFAC model built solely from these EEMS data, a recently developed peatland PARAFAC model based on pore water gathered from the Glacial Lake Agassiz peatlands (GLAP) in northern Minnesota (Tfaily et al., 2015) was used to analyze the EEMS spectra. This peatland had similar vegetation characteristics and DOM concentrations as those present at Stordalen. This model includes five components (Table A.1), with four (C1–C4) categorized as humic-like and one (C5) as protein-like. C1 likely represents plant-derived humic-like substances that can be biodegraded. C2 and C3 have shorter emission wavelengths than the other humic-like components, and thus appear to be microbially-derived, with C3 a possible microbial metabolite of C1. C4 appears refractory and likely represents either ubiquitous terrestrial high-molecular-weight humic-like aromatics, or terrestrial reduced quinones identified by Cory and McKnight (2005). The protein-like component, C5, corresponds with peak T as defined by Coble (1996) and is a marker for fresh (undecomposed) tryptophan-like structures.

The relative intensity of each component in the Stordalen samples was calculated by fitting the EEMS spectra to this PARAFAC model, with the loadings of each component interpreted as relative intensities in each sample. Detailed comparisons of PARAFAC component

intensities between Stordalen and the GLAP, as well as additional comparisons of elemental composition and optical properties, are given in the Supporting Information.

2.7.4. Statistical analysis of trends between samples

For each FT-ICR MS-derived value and optical property, as well as pH and DOC concentrations, one-way analyses of variance (ANOVA) were used to compare samples from different sites and habitat types. Since sampling only captured a few depths at each site (on each sampling date), depth trends were assessed with paired t-tests comparing the shallowest vs. the deepest samples in each depth profile that had at least two distinct depths. The results of these statistical tests are shown in Table 3.

2.7.5. Comparison of FT-ICR MS and optical measurements

To reveal general correlations between the FT-ICR MS and optical data, as well as the general trends in both datasets that separate different DOM samples, we performed two principal components analyses (PCA) with different combinations of FT-ICR MS and optical variables (Sleighter et al., 2010; Tfaily et al., 2015; Wagner et al., 2015). The first PCA examined general trends in elemental composition and optical properties without reference to compound class divisions or PARAFAC components, and included FT-ICR MS abundance-weighted average molecular characteristics (specifically, MW and element ratios) and non-PARAFAC optical properties (SUVA, BIX, HIX, Em_{max}, and F_{max}/A_{340}) . The second PCA examined interrelations between compound classes and PARAFAC components, and included FT-ICR MS compound class abundances and PARAFAC component relative intensities. Two separate PCAs were performed rather than combining all of the variables into one PCA in order to minimize autocorrelation between related sets of variables that were based on the same measurements (e.g., average O/C and tannin-like compound abundance). Both PCAs were performed with all variables scaled to unit variance to account for different measurement units and ranges of values.

Given that PCA may show misleading results due to dimensionality reduction, individual comparisons of each FT-ICR MS-derived variable (including compound classes as well as

419 average molecular characteristics) with each optical property across all samples represent a more
420 robust method for correlating molecular characteristics with optical properties. To this end, the
421 trends revealed by the PCAs were further explored and validated based on linear regressions,
422 with the bulk optical properties and PARAFAC component intensities as the independent
423 variables, and the FT-ICR MS results—including average molecular characteristics, total relative
424 abundance of each compound class, and total relative abundance of various combinations of up
425 to four compound classes—as the dependent variables. Combinations of compound classes were
426 chosen so that all classes occupied adjacent regions of the van Krevelen diagram and were not
427 surrounded on more than two sides by other compound classes (Fig. 1a).

428 ## 3. RESULTS

429 ### 3.1. DOC concentrations and pH

430 One-way ANOVAs (Table 3) revealed significant differences in both pH and DOC
431 concentrations between habitat types and between specific sites, with no significant differences
432 with depth (based on paired t-tests of shallow vs. deep samples; Table 3) or between sampling
433 dates (data not shown). Both pH and DOC mainly differed between rich fens and other sites
434 (collapsed palsas, bogs, and poor fens, which all had *Sphagnum*), with higher pH and much
435 lower DOC concentrations in rich fens (Table 1).

436 ### 3.2. FT-ICR MS

437 Based on van Krevelen and molecular size plots of all formulas, the overall elemental
438 compositions of bog and rich fen DOM were distinctly different, with lower O/C and higher H/C
439 (Fig. 1a) and lower molecular sizes (Fig. 1b) in rich fen DOM compared to bog DOM.

440 Across the entire thaw gradient, rich fens had a higher abundance of lipid-like, protein-
441 like, AS.carb, UH, and lignin-like compounds, as well as higher average H/C, N/C, and S/C,
442 while the sites with *Sphagnum* had more tannin-like compounds, higher O/C, and higher MW
443 (Fig. 2; exact values are given in Table A.2, and compound class abbreviations and ranges are

444 defined in Table 2). One-way ANOVAs (Table 3) revealed that these trends were significant for
445 the protein, AS.carb, lignin, and tannin compound classes. MW and O/C, H/C, and S/C also
446 varied significantly between habitat types, and O/C, H/C, N/C, and S/C varied significantly
447 between sites. Far fewer trends were observed with depth as compared with the trends between
448 sites and habitat types. Specifically, H/C and the AS.carb compound class both decreased with
449 depth in rich fens, while UH decreased with depth across all sites (Fig. 2, Table 3).

450 **3.3. Optical properties**

451 As with DOM elemental composition, most of the variation in optical properties
452 separated different sites and different habitat types (Table 3). Specifically, DOM from sites with
453 *Sphagnum* had higher SUVA, HIX, Em_{max}, and C1 and C4 relative intensities, while rich fens
454 had higher BIX, F_{max}/A_{340}, and C2 and C3 relative intensities (Fig. 3; exact values are given in
455 Table A.2, and terms are defined in the Methods, "2.7.2. Bulk optical properties" and "2.7.3.
456 PARAFAC model"). One-way ANOVAs revealed that all of these differences were significant
457 except for the differences in HIX (Table 3), likely because two of the *Sphagnum*-influenced
458 samples (Bog1.0.40 and EOS.0.38) had unusually low HIX (Fig. 3) due to high tryptophan-like
459 fluorescence. Fewer significant trends were observed with depth (Table 3). Among the depth
460 trends that were observed, C1 increased with depth across all sites, C1 and C5 increased with
461 depth in sites with *Sphagnum*, and Em_{max} increased with depth in rich fens (Fig. 3). No
462 significant differences were observed between sampling dates (data not shown).

463 **3.4. Correlation of optical properties with FT-ICR MS**

464 Both of the principal components analyses of variables measured in this study (Fig. 4)
465 showed a similar pattern in sample clustering in which rich fens are clearly separated from the
466 other sites along PC1, with higher PC1 scores in rich fens. In the first PCA (Fig. 4a), which
467 examined general trends in elemental composition and optical properties, PC1 correlates
468 positively with H/C, N/C, S/C, F_{max}/A_{340}, and BIX, and correlates negatively with O/C, MW,
469 Em_{max}, SUVA, and HIX. In the second PCA (Fig. 4b), which used more specific DOM

compound classes and PARAFAC components, PC1 correlates positively with the protein, AS.carb, lignin, lipid, and UH compound classes, as well as with PARAFAC components C2, C3, and C5, and correlates negatively with tannin-like compounds and PARAFAC components C1 and C4. PC2 explained a small proportion of the variance in both PCAs (14% and 15%, respectively), and components PC2 and above showed no significant relationships with habitat type, site, or depth. This large proportion of unexplained variance (48% in Fig. 4a and 58% in Fig. 4b, since only PC1 was related to sample characteristics) is likely due to charge competition in FT-ICR MS, which results in nonlinear responses of observed compound relative abundances relative to true compound concentrations.

Results of linear regressions between FT-ICR MS results (including compound classes, as well as average molecular characteristics across the entire spectra) and non-PARAFAC optical properties are shown in Table A.3, and regressions between FT-ICR MS results and PARAFAC component intensities are shown in Table A.4. The FT-ICR MS variables with the strongest correlations with each non-PARAFAC optical property (Table A.3) were all spectra-averaged molecular characteristics rather than compound class abundances. Among the PARAFAC components, all components except C5 showed significant relationships with FT-ICR MS data (Table A.4). More detailed summaries of these results are provided in the Discussion.

4. DISCUSSION

4.1. Differences in elemental composition between bogs and rich fens

Van Krevelen and molecular size difference plots of Stordalen bog and rich fen samples from a range of depths (10–70 cm for bogs and 7–70 cm for fens) indicate higher H/C, lower O/C, and lower molecular sizes in rich fens compared to bogs (Fig. 1). Similar differences are observed across the whole range of bog and rich fen samples (Fig. 2), including those not included in the more detailed plots shown in Fig. 1. These results extend a previous comparison of single bog and rich fen samples from ~30 cm (specifically, samples SOS.1.31 and E.1.26;

Hodgkins et al., 2014) to six bog and six rich fen samples spanning five sites and a broad range of depths (Table 1).

4.2. Bulk optical properties are consistent with elemental composition

Based on linear regressions (Table A.3), most of the measured optical properties showed trends that were consistent with the elemental composition parameters that are expected from the types of molecules identified. This was despite the possibility of matrix effects affecting DOM optical properties (Sharpless and Blough, 2014). Although all of the samples were freshwater and likely had similar redox states (few differences were observed with depth; Table 3), pH differences between site types (Table 1) could have affected the differences in optical properties observed here (Tfaily et al., 2011; pH differences were unlikely to have affected FT-ICR MS results because all samples were acidified to pH = 2 prior to extraction). These caveats highlight the importance of using both methods (elemental composition and optical properties) when evaluating differences in DOM chemistry between samples.

Consistent with Stewart and Wetzel's (1981) finding that the fluorescence/absorbance ratio of DOM correlates negatively with MW, F_{max}/A_{340} of our samples was negatively correlated with average MW, representing the strongest correlation for this optical property ($R^2 = 0.27$, $p = 0.006$; Table A.3). Optical properties also generally predicted DOM aromaticity, but with more ambiguous results. Based on SUVA, Em_{max}, BIX, HIX, and H/C (Figs. 2, 3, and 4a), sites with *Sphagnum* appear to contain more aromatic structures. However, the condensed aromatic (CA) compound class did not appear to show any variation between different site types (Fig. 2, Table 3), likely because it contributes little to the DOM composition observed with negative ESI (Figs. 1a and 2). CA also did not correlate with most of the optical properties, except for the expected positive correlation with SUVA ($R^2 = 0.22$, $p = 0.01$; Table A.3), suggesting that the trends in the other optical properties related to aromaticity (Em_{max}, BIX, and HIX) are due to changes in other compounds. In contrast to CA, abundance-weighted average H/C and (H+O)/C, which both increase with decreasing aromaticity (the better-correlated ratio depends on whether O is

predominately bonded to C by single or double bonds), were both strongly negatively correlated with SUVA, Em_{max}, and BIX (Table A.3). These results suggest one (or both) of two conclusions. The most condensed aromatic structures, represented by the CA class, may not be easily measured by FT-ICR MS with negative ESI, likely due to their relative lack of ionizable carboxylic acid groups. Alternately, the overall aromaticity of DOM at Stordalen may be dominated by compounds with a moderate degree of aromaticity (such as lignin- and tannin-like compounds) rather than by highly condensed polyaromatic compounds (represented by the CA class).

Both PCAs—the first analyzing average molecular characteristics (Sleighter et al., 2010; Wagner et al., 2015) and bulk optical properties (Tfaily et al., 2015) (Fig. 4a), and the second analyzing compound class abundances and PARAFAC components (Tfaily et al., 2015) (Fig. 4b) —show a similarity in sample clustering in which rich fens are clearly separated from the other sites along PC1. This result highlights the robustness of both methods of measuring DOM elemental composition (average molecular characteristics vs. compound class abundances) and of both methods of measuring optical properties (commonly applied indices of SUVA, BIX, HIX, Em_{max}, and F_{max}/A_{340}, vs. PARAFAC components). Thus, if any artefacts were caused by the compound class boundaries (which cannot be precisely defined) or PARAFAC components (which were defined based on data from a different peatland), these effects were likely minimal.

4.3. Possible identities of PARAFAC components

Probable compound class assignments for the PARAFAC components were determined based on the strongest positive linear correlations (Table A.4) with each single compound class defined for FT-ICR MS data (shown in Table 2 and Fig. 1a), as well as with various combinations of adjacent compound classes. In correlations of compound class abundances with PARAFAC components, a positive correlation can be interpreted more easily than a negative correlation because it suggests that both measures may represent the same set of compounds. Although these correlations do not provide absolute proof that the compound classes and

PARAFAC components represent equivalent sets of compounds, the best-correlated sets of compounds are consistent with the properties expected for each component (Table A.1). Specifically, both C1 and C4 correlate best with a combination of CA and tannin-like compounds, which are more likely to be found in plant-derived DOM. In contrast, C2 correlates best with AS.carb compounds, while C3 correlates best with a combination of lipid, protein, AS.carb, and UH compounds, all of which have higher H/C consistent with microbial production. C5 did not correlate with any compound classes identifiable by FT-ICR MS (Table A.4), possibly because this region of the spectrum can be associated not just with proteins (more abundant in rich fens), but also with polyphenols such as tannins (more abundant in sites with *Sphagnum*) (Maie et al., 2007; Hernes et al., 2009; Yamashita et al., 2011).

Across all samples, there was a strong negative correlation between the abundances of C1 and C3 ($R^2 = 0.92$, $p < 0.0001$; Fig. 5). This result is consistent with the trends in C1 and C3 in the GLAP, where C1 decreased with depth while C3 increased, and suggests that the degradation of C1 may be associated with microbial production of C3 (Tfaily et al., 2015).

Similar to peatland pore water, microbial processing in lakes and rivers tends to drive PARAFAC component intensities toward fluorophores with shorter emission wavelengths; however, differences are often observed from peatland DOM in the exact excitation and emission wavelengths and overall shapes of the components (Mann et al., 2012; Walker et al., 2013; Kellerman et al., 2015). These differences could be caused by the following: (a) photobleaching in open water, which would not occur in subsurface peat pore water; (b) different pathways of DOM degradation under aerobic (open water) and anaerobic (peat pore water) conditions; and/or (c) contribution of algal-derived DOM to fluorescence in open water. In addition to these effects, the PARAFAC approach itself may also yield components that cannot be directly compared between environments. The assumption within PARAFAC that different species fluoresce independently is questionable, given that DOM fluorescence properties are influenced by charge transfer interactions between different fluorophores, dissolved ions (including pH differences), and dissolved oxygen (Sharpless and Blough, 2014). It is thus important to note that the

574 correlations between compound classes and PARAFAC components described here are merely
575 co-occurrences, and should not be interpreted as direct structural assignments.

576 **4.4. *Sphagnum* is a primary driver of DOM properties**

577 Based on two separate PCAs using a wide range optical properties and elemental
578 composition data (Fig. 4), rich fens are clearly separated from the other sites, with no systematic
579 trends between the remaining site types (collapsed palsa, bog, and poor fen) that have *Sphagnum*
580 as a dominant plant species. Although a few depth trends were observed (Table 3), these trends
581 are generally weak, as they were not consistently observed over the entire depth range in profiles
582 with >2 depths (Figs. 2 and 3), and none of the principal components showed significant
583 correlations with depth. This result suggests that the presence or absence of dense *Sphagnum* is
584 the main driver of DOM elemental composition and optical properties at Stordalen. This
585 interpretation is consistent with the much higher DOC concentrations in sites with *Sphagnum*
586 (Table 1), which are likely due to the accumulation of recalcitrant organic compounds released
587 by *Sphagnum* (Chanton et al., 2008).

588 DOM in sites with *Sphagnum* had a higher relative abundance of tannin-like and other
589 high-O/C compounds compared to rich fens (Figs. 2 and 4). These compounds may represent
590 *Sphagnum*-derived phenolics that could contribute to the suppression of decomposition at these
591 sites (Verhoeven and Toth, 1995; van Breemen, 1995; Verhoeven and Liefveld, 1997; Freeman
592 et al., 2004). In contrast, the more saturated, lower-oxygen compounds in rich fens may reflect
593 the lower release of phenolics by sedges compared to *Sphagnum*, while the higher N/C and S/C
594 in rich fens (Figs. 2 and 4a) may be driven by the higher N and S content of vascular plants
595 (Hornibrook et al., 2000). *Sphagnum*-derived acidic carbohydrates (e.g., sphagnan), which would
596 fall into the AS.carb class and are thought to suppress decomposition (Painter, 1983, 1991), had
597 very low observed abundance in all sites (Figs. 1a and 2). The low observed abundance of
598 AS.carb compounds was likely due to their high polarity, which would have prevented their
599 extraction with PPL cartridges.

The higher abundance of high-oxygen tannin-like compounds, which are likely to include phenolic moieties, in sites with *Sphagnum* than in rich fens, is consistent with the enzymatic latch mechanism (Freeman et al., 2001) proposed for keeping DOC concentrations high and decomposition rates low at sites with *Sphagnum*. According to this mechanism, the phenolics that inhibit decomposition are degraded by phenol oxidase, and this enzyme is inhibited by anaerobic conditions (Freeman et al., 2001, 2004) and by acidic pH (Williams et al., 2000; Tahvanainen and Haraguchi, 2013; Xiang et al., 2013). The more acidic pH of the sites with *Sphagnum* (Table 1) may thus protect phenolic compounds from decomposition by inhibiting phenol oxidase, and these phenolics may then inhibit the degradation of other compounds. Complexation of phenol oxidase with sphagnan or sphagnum acid represents one possible mechanism for its inhibition under acidic conditions, such that this enzyme may be inhibited by these specific acids rather than by pH alone. Since slow decomposition would prevent the degradation of these organic acids, the buildup of these acids, and the resulting inhibition of phenol oxidase and subsequent buildup of phenolics, may represent a self-amplifying feedback mechanism in which each compound group (*Sphagnum*-derived acids and phenolics) builds up due to the presence of the other. Both of these compound groups may then inhibit overall decomposition rates at sites with *Sphagnum*.

4.5. Microbial activity influences rich fen DOM composition

The DOM optical properties suggest that compared to the other sites, DOM from rich fens likely includes a higher proportion of microbially-produced material. Although all BIX values were <0.6, indicating that the majority of DOM in all samples was plant-derived, the higher BIX values in rich fens (Figs. 3 and 4a) suggest a higher contribution of microbially-derived DOM in these sites compared to the sites with *Sphagnum* (Huguet et al., 2009). This finding is consistent with those of Hodgkins et al. (2014), who observed higher rates of decomposition in rich fen peat compared to collapsed palsa, bog, and poor fen peat. PARAFAC components C2 and C3, which likely represent microbially-derived material (Tfaily et al., 2015),

626 also had higher relative intensities in rich fens compared to the other sites (Figs. 3 and 4b). We
627 can thus assume that the higher BIX and slightly lower HIX values in rich fens (Figs. 3 and 4a)
628 indicate greater production of microbially-derived material (Kalbitz et al., 2003b; Birdwell and
629 Engel, 2010; Tfaily et al., 2015) rather than a lower degree of DOM humification. However, the
630 difference in HIX between sites was not significant (Table 3), indicating possible contribution of
631 DOM humification to the variability in HIX between samples (Kalbitz et al., 2003b).
632 Given that microorganisms in peat are known to immobilize N in their biomass
633 (Damman, 1988), the higher N/C in rich fens (Figs. 2 and 4a) may reflect higher microbial
634 activity in addition to higher N/C from plant inputs at these sites. This possibility is supported by
635 the correlation of higher N/C with optical properties indicative of microbially-produced DOM
636 (specifically, positive correlations with BIX, C2, and C3, and negative correlations with Em_{max}
637 and C1; Tables A.3 and A.4). This mechanism may amplify the effects of plant input on N/C
638 (Hornibrook et al., 2000), as the comparatively N-rich DOM produced by sedges in rich fens
639 would be further N-enriched by preferential microbial assimilation of N, followed by release of
640 N-rich DOM from microbes via secretion and cell lysis. Given that S/C was also higher in rich
641 fens (Figs. 2 and 4a) and was correlated with optical properties associated with microbial DOM
642 (including all optical properties correlated with N/C, as well as negative correlations with SUVA
643 and HIX; Tables A.3 and A.4), S enrichment may also occur by a similar mechanism (Novák et
644 al., 1999). Although PCA showed a spread in rich fens along PC2 (Fig. 4a) in which some
645 samples (E.1.26, E.2.7, and E.2.70) were specifically enriched in S/C while the remaining
646 samples were specifically enriched in N/C, there is little evidence that these differences are
647 related to site or depth.
648 The lower MW of rich fen DOM, as indicated by both average MW and F_{max}/A_{340}, may
649 reflect more advanced decomposition at these sites. In the size-reactivity model (Amon and
650 Benner, 1996; Burdige and Gardner, 1998) (summarized in "1.2. Controls on DOM composition
651 and lability"), HMW-DOM is broken down into LMW-DOM, with the cutoff between these size
652 classes defined at either 1000 Da or 3000 Da. Within the LMW-DOM size class, the effects of

653 decomposition are generally more varied, with some studies reporting a decrease in molecular
654 size with decomposition (e.g., Kalbitz et al., 2003b; Tfaily et al., 2013, 2015) while others report
655 an increase (e.g., Gruber et al., 2006; Hur, 2011). Although the mass range measured in this
656 study (m/z = 170 to 800 Da) falls entirely within the LMW-DOM size class, the association of
657 lower MW with optical properties indicative of higher microbial activity (BIX, C2, and C3;
658 Tables A.3 and A.4) suggests that the size reactivity model may apply to decomposition of the
659 LMW-DOM pool in peatlands. Specifically, the smaller DOM molecules found in rich fens may
660 reflect mLMW-DOM and/or pLMW-DOM that is partially degraded into mLMW-DOM, while
661 the larger molecules found in sites with *Sphagnum* may reflect less degraded, more recalcitrant
662 pLMW-DOM. In rich fens, more efficient decomposition of pLMW-DOM may be enabled by a
663 greater diversity of reactions encoded by a more diverse microbial community (Mondav et al.,
664 2014), which would increase the number of possible pathways for DOM degradation.

665 Our results complement and are consistent with those of Kellerman et al. (2015), who
666 used a combination of FT-ICR MS and optical properties to examine DOM from 109 Swedish
667 lakes spanning a wide range of climates and catchments. Kellerman et al. (2015) found that
668 DOM from lakes with longer water residence times (and thus more autochthonous DOM
669 production) had a lower oxidation state, lower aromaticity, smaller apparent MW, and higher N
670 and S content compared to DOM from lakes with a stronger terrestrial influence. Our data
671 suggests that transition from partially-thawed peatlands with abundant *Sphagnum* to fully-thawed
672 rich fens with little *Sphagnum* may result in similar changes in DOM composition as observed in
673 lakes with long water residence times, with both leading to an increased proportion of
674 microbially-produced DOM.

675 **5. CONCLUSIONS**

676 Using a combination of ultrahigh resolution mass spectrometry and comprehensive
677 analysis of fluorescence spectra, we found consistent patterns in DOM chemistry across a variety
678 of peatland types at Stordalen Mire. In partially to fully waterlogged sites at Stordalen, the

679 presence of dense *Sphagnum* moss appears to control DOM composition, such that DOM in sites
680 with *Sphagnum* contains more aromatic, higher-oxygen, and higher-MW compounds. Some of
681 these compounds, particularly tannin-like phenolics, may accumulate due to the inhibition of
682 phenol oxidase by acidic pH. In conjunction with sphagnan and other inhibitory compounds,
683 these phenolics then slow decomposition rates at sites with *Sphagnum*, keeping DOC
684 concentrations high while reducing the rate of carbon release as CH_4 and CO_2. Conversely, in
685 rich fens that contain little to no living *Sphagnum*, DOM has lower aromaticity and greater N/C
686 and S/C consistent with more microbially-derived material. This result is consistent with Ward
687 and Cory's (2015) finding that lower aromatic content in permafrost DOM is associated with
688 higher bacterial growth. At Stordalen, the higher rates of microbial activity in rich fens translate
689 into greater CH_4 and CO_2 production at these sites (Hodgkins et al., 2014).
690 Taken together, these results indicate that DOM optical properties and elemental
691 composition at Stordalen Mire vary mostly along a plant community succession associated with
692 permafrost thaw (Johansson et al., 2006; Mondav et al., 2014; Hodgkins et al., 2014; McCalley
693 et al., 2014), specifically the presence or absence of abundant *Sphagnum* that appears in the
694 earlier thaw stages. In this way, *Sphagnum* acts as a "keystone" genus that disproportionately
695 controls the biodegradability of DOM. Because *Sphagnum* and its litter in peat soils are thought
696 to store more carbon than any other plant genus (Clymo and Hayward, 1982), any effects of
697 climate change on this plant's distribution, and consequent changes in DOM lability, could have
698 major ramifications on a global scale. This is especially true at Arctic and boreal latitudes, which
699 have more *Sphagnum* and are warming more rapidly than temperate and tropical latitudes. In
700 permafrost peatlands with similar thaw successions as Stordalen, shifts from *Sphagnum*-
701 dominated sites with thawing permafrost to fully-thawed rich fens without *Sphagnum* may lead
702 to enhanced biodegradability of peatland DOM, and hence greater CH_4 emissions. Conversely, in
703 areas where warming leads to the expansion of *Sphagnum* bogs, a negative climate feedback may
704 result from increased carbon accumulation and lower CH_4 emissions (Tolonen and Turunen,
705 1996). Larger scale estimations of the prevalence of Stordalen-like thaw sequences in other

Arctic wetlands may help to determine the global significance and direction of this warming feedback.

ACKNOWLEDGEMENTS

This research was funded by the US Department of Energy Office of Biological and Environmental Research under the Genomic Science program (Awards DE-SC0004632 and DE-SC0010580). Infrastructure for sampling was provided by the Abisko Scientific Research Station, and mass spectra were obtained at the National High Magnetic Field Laboratory FT-ICR Facility in Tallahassee, FL (Project NSF DMR-1157490). David Podgorski received support from the FSU Future Fuels Institute. Scott Saleska and Virginia Rich received additional support through the Ecosystem Genomics Initiative from the University of Arizona Technology and Research Initiative Fund, via the program in Water, Environmental and Energy Solutions.

APPENDIX A: SUPPLEMENTARY DATA

Supplementary data associated with this article, including detailed comparisons between Stordalen and the GLAP samples used to produce the PARAFAC model, can be found in the online version.

REFERENCES

Alperin M. J., Albert D. B. and Martens C. S. (1994) Seasonal variations in production and consumption rates of dissolved organic carbon in an organic-rich coastal sediment. *Geochim. Cosmochim. Acta* **58**, 4909–4930.

Amon R. M. W. and Benner R. (1996) Bacterial utilization of different size classes of dissolved organic matter. *Limnol. Oceanogr.* **41**, 41–51.

Bäckstrand K., Crill P. M., Jackowicz-Korczyñski M., Mastepanov M., Christensen T. R. and Bastviken D. (2010) Annual carbon gas budget for a subarctic peatland, Northern Sweden. *Biogeosciences* **7**, 95–108.

Baker A., Tipping E., Thacker S. A. and Gondar D. (2008) Relating dissolved organic matter fluorescence and functional properties. *Chemosphere* **73**, 1765–1772.

732 Birdwell J. E. and Engel A. S. (2010) Characterization of dissolved organic matter in cave and
733 spring waters using UV–Vis absorbance and fluorescence spectroscopy. *Org. Geochem.*
734 **41**, 270–280.

735 Blodau C. and Deppe M. (2012) Humic acid addition lowers methane release in peats of the Mer
736 Bleue bog, Canada. *Soil Biol. Biochem.* **52**, 96–98.

737 van Breemen N. (1995) How *Sphagnum* bogs down other plants. *Trends Ecol. Evol.* **10**, 270–
738 275.

739 Bridgham S. D., Cadillo-Quiroz H., Keller J. K. and Zhuang Q. (2013) Methane emissions from
740 wetlands: biogeochemical, microbial, and modeling perspectives from local to global
741 scales. *Glob. Change Biol.* **19**, 1325–1346.

742 Brown T. L. and Rice J. A. (2000) Effect of experimental parameters on the ESI FT-ICR mass
743 spectrum of fulvic acid. *Anal. Chem.* **72**, 384–390.

744 Burdige D. J. and Gardner K. G. (1998) Molecular weight distribution of dissolved organic
745 carbon in marine sediment pore waters. *Mar. Chem.* **62**, 45–64.

746 Cervantes F. J., van der Velde S., Lettinga G. and Field J. A. (2000) Competition between
747 methanogenesis and quinone respiration for ecologically important substrates in
748 anaerobic consortia. *FEMS Microbiol. Ecol.* **34**, 161–171.

749 Chanton J. P., Glaser P. H., Chasar L. S., Burdige D. J., Hines M. E., Siegel D. I., Tremblay L.
750 B. and Cooper W. T. (2008) Radiocarbon evidence for the importance of surface
751 vegetation on fermentation and methanogenesis in contrasting types of boreal peatlands.
752 *Glob. Biogeochem. Cycles* **22**, GB 4022.

753 Christensen T. R., Johansson T., Åkerman H. J., Mastepanov M., Malmer N., Friborg T., Crill P.
754 and Svensson B. H. (2004) Thawing sub-arctic permafrost: Effects on vegetation and
755 methane emissions. *Geophys. Res. Lett.* **31**, L04501.

756 Clymo R. S. and Hayward P. M. (1982) The ecology of *Sphagnum*. In *Bryophyte Ecology* (ed. A.
757 J. E. Smith). Chapman and Hall, New York, NY. pp. 229–289.

758 Coble P. G. (1996) Characterization of marine and terrestrial DOM in seawater using excitation-
759 emission matrix spectroscopy. *Mar. Chem.* **51**, 325–346.

760 Coble P. G., Del Castillo C. E. and Avril B. (1998) Distribution and optical properties of CDOM
761 in the Arabian Sea during the 1995 Southwest Monsoon. *Deep Sea Res. Part II Top. Stud.*
762 *Oceanogr.* **45**, 2195–2223.

763 Cory R. M. and McKnight D. M. (2005) Fluorescence spectroscopy reveals ubiquitous presence
764 of oxidized and reduced quinones in dissolved organic matter. *Environ. Sci. Technol.* **39**,
765 8142–8149.

766 Damman A. W. H. (1988) Regulation of nitrogen removal and retention in Sphagnum bogs and
767 other peatlands. *Oikos* **51**, 291–305.

768 Dittmar T., Koch B., Hertkorn N. and Kattner G. (2008) A simple and efficient method for the
769 solid-phase extraction of dissolved organic matter (SPE-DOM) from seawater. *Limnol.*
770 *Oceanogr. Methods* **6**, 230–235.

771 Forster P., Ramaswamy V., Artaxo P., Bernsten T., Betts R., Fahey D. W., Haywood J., Lean J.,
772 Lowe D. C., Myhre G., Nganga J., Prinn R., Raga G., Schulz M. and Van Dorland R.
773 (2007) Changes in atmospheric constituents and in radiative forcing. In *Climate Change*
774 *2007: The Physical Science Basis. Contribution of Working Group I to the Fourth*
775 *Assessment Report of the Intergovernmental Panel on Climate Change* (eds. S. Solomon,
776 D. Qin, M. Manning, Z. Chen, M. Marquis, K. B. Averyt, M. Tignor, and H. L. Miller).
777 Cambridge University Press, Cambridge, UK. pp. 129–234. Available at:
778 http://www.ipcc.ch/pdf/assessment-report/ar4/wg1/ar4-wg1-chapter2.pdf [Accessed
779 December 5, 2012].

780 Freeman C., Ostle N. J., Fenner N. and Kang H. (2004) A regulatory role for phenol oxidase
781 during decomposition in peatlands. *Soil Biol. Biochem.* **36**, 1663–1667.

782 Freeman C., Ostle N. and Kang H. (2001) An enzymic "latch" on a global carbon store: A
783 shortage of oxygen locks up carbon in peatlands by restraining a single enzyme. *Nature*
784 **409**, 149–149.

785 Glatzel S., Kalbitz K., Dalva M. and Moore T. (2003) Dissolved organic matter properties and
786 their relationship to carbon dioxide efflux from restored peat bogs. *Geoderma* **113**, 397–
787 411.

788 Gonsior M., Peake B. M., Cooper W. J., Jaffé R., Young H., Kahn A. E. and Kowalczuk P.
789 (2008) Spectral characterization of chromophoric dissolved organic matter (CDOM) in a
790 fjord (Doubtful Sound, New Zealand). *Aquat. Sci.* **70**, 397–409.

791 Gorham E. (1991) Northern peatlands: Role in the carbon cycle and probable responses to
792 climatic warming. *Ecol. Appl.* **1**, 182–195.

793 Gruber D. F., Simjouw J.-P., Seitzinger S. P. and Taghon G. L. (2006) Dynamics and
794 characterization of refractory dissolved organic matter produced by a pure bacterial
795 culture in an experimental predator-prey system. *Appl. Environ. Microbiol.* **72**, 4184–
796 4191.

797 Harvey H. R., Tuttle J. H. and Bell J. T. (1995) Kinetics of phytoplankton decay during
798 simulated sedimentation: Changes in biochemical composition and microbial activity
799 under oxic and anoxic conditions. *Geochim. Cosmochim. Acta* **59**, 3367–3377.

800 Heitmann T., Goldhammer T., Beer J. and Blodau C. (2007) Electron transfer of dissolved
801 organic matter and its potential significance for anaerobic respiration in a northern bog.
802 *Glob. Change Biol.* **13**, 1771–1785.

803 Hernes P. J., Bergamaschi B. A., Eckard R. S. and Spencer R. G. M. (2009) Fluorescence-based
804 proxies for lignin in freshwater dissolved organic matter. *J. Geophys. Res.* **114**, G00F03.

805 Hodgkins S. B., Tfaily M. M., McCalley C. K., Logan T. A., Crill P. M., Saleska S. R., Rich V.
806 I. and Chanton J. P. (2014) Changes in peat chemistry associated with permafrost thaw
807 increase greenhouse gas production. *Proc. Natl. Acad. Sci. U. S. A.* **111**, 5819–5824.

808 Hornibrook E. R. C., Longstaffe F. J., Fyfe W. S. and Bloom Y. (2000) Carbon-isotope ratios
809 and carbon, nitrogen and sulfur abundances in flora and soil organic matter from a
810 temperate-zone bog and marsh. *Geochem. J.* **34**, 237–245.

811 Huguet A., Vacher L., Relexans S., Saubusse S., Froidefond J. M. and Parlanti E. (2009)
812 Properties of fluorescent dissolved organic matter in the Gironde Estuary. *Org. Geochem.*
813 **40**, 706–719.

814 Hur J. (2011) Microbial changes in selected operational descriptors of dissolved organic matters
815 from various sources in a watershed. *Water. Air. Soil Pollut.* **215**, 465–476.

816 Ishii S. K. L. and Boyer T. H. (2012) Behavior of reoccurring PARAFAC components in
817 fluorescent dissolved organic matter in natural and engineered systems: A critical review.
818 *Environ. Sci. Technol.* **46**, 2006–2017.

819 Johansson T., Malmer N., Crill P. M., Friborg T., Åkerman J. H., Mastepanov M. and
820 Christensen T. R. (2006) Decadal vegetation changes in a northern peatland, greenhouse
821 gas fluxes and net radiative forcing. *Glob. Change Biol.* **12**, 2352–2369.

822 Kalbitz K., Schmerwitz J., Schwesig D. and Matzner E. (2003a) Biodegradation of soil-derived
823 dissolved organic matter as related to its properties. *Geoderma* **113**, 273–291.

824 Kalbitz K., Schwesig D., Schmerwitz J., Kaiser K., Haumaier L., Glaser B., Ellerbrock R. and
825 Leinweber P. (2003b) Changes in properties of soil-derived dissolved organic matter
826 induced by biodegradation. *Soil Biol. Biochem.* **35**, 1129–1142.

827 Keller J. K. and Bridgham S. D. (2007) Pathways of anaerobic carbon cycling across an
828 ombrotrophic-minerotrophic peatland gradient. *Limnol. Oceanogr.* **52**, 96–107.

829 Kellerman A. M., Kothawala D. N., Dittmar T. and Tranvik L. J. (2015) Persistence of dissolved
830 organic matter in lakes related to its molecular characteristics. *Nat. Geosci.* **8**, 454–457.

831 Kim S., Kramer R. W. and Hatcher P. G. (2003) Graphical method for analysis of ultrahigh-
832 resolution broadband mass spectra of natural organic matter, the van Krevelen diagram.
833 *Anal. Chem.* **75**, 5366–5344.

834 Kindler R., Miltner A., Richnow H.-H. and Kästner M. (2006) Fate of gram-negative bacterial
835 biomass in soil—mineralization and contribution to SOM. *Soil Biol. Biochem.* **38**, 2860–
836 2870.

837 Kindler R., Miltner A., Thullner M., Richnow H.-H. and Kästner M. (2009) Fate of bacterial
838 biomass derived fatty acids in soil and their contribution to soil organic matter. *Org.*
839 *Geochem.* **40**, 29–37.

840 Kirk T. K. and Farrell R. L. (1987) Enzymatic "combustion": The microbial degradation of
841 lignin. *Annu. Rev. Microbiol.* **41**, 465–505.

842 Kögel-Knabner I. (2002) The macromolecular organic composition of plant and microbial
843 residues as inputs to soil organic matter. *Soil Biol. Biochem.* **34**, 139–162.

844 Kowalczuk P., Cooper W. J., Whitehead R. F., Durako M. J. and Sheldon W. (2003)
845 Characterization of CDOM in an organic-rich river and surrounding coastal ocean in the
846 South Atlantic Bight. *Aquat. Sci.* **65**, 384–401.

847 Kujawinski E. B., Hatcher P. G. and Freitas M. A. (2002) High-resolution Fourier transform ion
848 cyclotron resonance mass spectrometry of humic and fulvic acids: improvements and
849 comparisons. *Anal. Chem.* **74**, 413–419.

850 Lawaetz A. J. and Stedmon C. A. (2009) Fluorescence intensity calibration using the Raman
851 scatter peak of water. *Appl. Spectrosc.* **63**, 936–940.

852 Lorenz K., Lal R., Preston C. M. and Nierop K. G. J. (2007) Strengthening the soil organic
853 carbon pool by increasing contributions from recalcitrant aliphatic bio(macro)molecules.
854 *Geoderma* **142**, 1–10.

855 Lovley D. R., Coates J. D., Blunt-Harris E. L., Phillips E. J. P. and Woodward J. C. (1996)
856 Humic substances as electron acceptors for microbial respiration. *Nature* **382**, 445–448.

857 Maie N., Scully N. M., Pisani O. and Jaffé R. (2007) Composition of a protein-like fluorophore
858 of dissolved organic matter in coastal wetland and estuarine ecosystems. *Water Res.* **41**,
859 563–570.

860 Malmer N., Johansson T., Olsrud M. and Christensen T. R. (2005) Vegetation, climatic changes
861 and net carbon sequestration in a North-Scandinavian subarctic mire over 30 years. *Glob.*
862 *Change Biol.* **11**, 1895–1909.

863 Mann P. J., Davydova A., Zimov N., Spencer R. G. M., Davydov S., Bulygina E., Zimov S. and
864 Holmes R. M. (2012) Controls on the composition and lability of dissolved organic
865 matter in Siberia's Kolyma River basin. *J. Geophys. Res.* **117**, G01028.

866 Marschner B. and Kalbitz K. (2003) Controls of bioavailability and biodegradability of dissolved
867 organic matter in soils. *Geoderma* **113**, 211–235.

868 McCalley C. K., Woodcroft B. J., Hodgkins S. B., Wehr R. A., Kim E.-H., Mondav R., Crill P.
869 M., Chanton J. P., Rich V. I., Tyson G. W. and Saleska S. R. (2014) Methane dynamics
870 regulated by microbial community response to permafrost thaw. *Nature* **514**, 478–481.

McGuire A. D., Anderson L. G., Christensen T. R., Dollimore S., Guo L., Hayes D. J., Heimann M., Lorenson T. D., Macdonald R. W. and Roulet N. (2009) Sensitivity of the carbon cycle in the Arctic to climate change. *Ecol. Monogr.* **79**, 523–555.

Miltner A., Kindler R., Knicker H., Richnow H.-H. and Kästner M. (2009) Fate of microbial biomass-derived amino acids in soil and their contribution to soil organic matter. *Org. Geochem.* **40**, 978–985.

Mondav R., Woodcroft B. J., Kim E.-H., McCalley C. K., Hodgkins S. B., Crill P. M., Chanton J., Hurst G. B., VerBerkmoes N. C., Saleska S. R., Hugenholtz P., Rich V. I. and Tyson G. W. (2014) Discovery of a novel methanogen prevalent in thawing permafrost. *Nat. Commun.* **5**, 3212.

Novák M., Buzek F. and Adamová M. (1999) Vertical trends in $\delta^{13}C$, $\delta^{15}N$ and $\delta^{34}S$ ratios in bulk *Sphagnum* peat. *Soil Biol. Biochem.* **31**, 1343–1346.

Ogawa H., Amagai Y., Koike I., Kaiser K. and Benner R. (2001) Production of refractory dissolved organic matter by bacteria. *Science* **292**, 917–920.

Painter T. J. (1983) Carbohydrate origin of aquatic humus from peat. *Carbohydr. Res.* **124**, C22–C26.

Painter T. J. (1991) Lindow Man, Tollund Man and other peat-bog bodies: The preservative and antimicrobial action of sphagnan, a reactive glycuronoglycan with tanning and sequestering properties. *Carbohydr. Polym.* **15**, 123–142.

Rausch N., Ukonmaanaho L., Nieminen T. M., Krachler M., Roux G. L. and Shotyk W. (2006) Evaluation of samplers and filter materials for the establishment of trace metal concentration profiles in peat bog porewaters using inductively coupled plasma-mass spectrometry. *Anal. Chim. Acta* **558**, 201–210.

Schuur E. A. G., Bockheim J., Canadell J. G., Euskirchen E., Field C. B., Goryachkin S. V., Hagemann S., Kuhry P., Lafleur P. M., Lee H., Mazhitova G., Nelson F. E., Rinke A., Romanovsky V. E., Shiklomanov N., Tarnocai C., Venevsky S., Vogel J. G. and Zimov S. A. (2008) Vulnerability of permafrost carbon to climate change: implications for the global carbon cycle. *BioScience* **58**, 701–714.

Senesi N. (1990) Molecular and quantitative aspects of the chemistry of fulvic acid and its interactions with metal ions and organic chemicals: Part II. The fluorescence spectroscopy approach. *Anal. Chim. Acta* **232**, 77–106.

Sharpless C. M. and Blough N. V. (2014) The importance of charge-transfer interactions in determining chromophoric dissolved organic matter (CDOM) optical and photochemical properties. *Environ. Sci. Process. Impacts* **16**, 654–671.

Shindell D. T., Faluvegi G., Koch D. M., Schmidt G. A., Unger N. and Bauer S. E. (2009) Improved attribution of climate forcing to emissions. *Science* **326**, 716–718.

907 Sleighter R. L., Chen H., Wozniak A. S., Willoughby A. S., Caricasole P. and Hatcher P. G.
908 (2012) Establishing a measure of reproducibility of ultrahigh-resolution mass spectra for
909 complex mixtures of natural organic matter. *Anal. Chem.* **84**, 9184–9191.

910 Sleighter R. L. and Hatcher P. G. (2007) The application of electrospray ionization coupled to
911 ultrahigh resolution mass spectrometry for the molecular characterization of natural
912 organic matter. *J. Mass Spectrom.* **42**, 559–574.

913 Sleighter R. L., Liu Z., Xue J. and Hatcher P. G. (2010) Multivariate statistical approaches for
914 the characterization of dissolved organic matter analyzed by ultrahigh resolution mass
915 spectrometry. *Environ. Sci. Technol.* **44**, 7576–7582.

916 Stedmon C. A. and Bro R. (2008) Characterizing dissolved organic matter fluorescence with
917 parallel factor analysis: a tutorial. *Limnol. Oceanogr. Methods* **6**, 572–579.

918 Stenson A. C., Marshall A. G. and Cooper W. T. (2003) Exact masses and chemical formulas of
919 individual Suwannee River fulvic acids from ultrahigh resolution electrospray ionization
920 Fourier transform ion cyclotron resonance mass spectra. *Anal. Chem.* **75**, 1275–1284.

921 Stewart A. J. and Wetzel R. G. (1981) Asymmetrical relationships between absorbance,
922 fluorescence, and dissolved organic carbon. *Limnol. Oceanogr.* **26**, 590–597.

923 Stubbins A., Lapierre J.-F., Berggren M., Prairie Y. T., Dittmar T. and del Giorgio P. A. (2014)
924 What's in an EEM? Molecular signatures associated with dissolved organic fluorescence
925 in boreal Canada. *Environ. Sci. Technol.* **48**, 10598–10606.

926 Tahvanainen T. and Haraguchi A. (2013) Effect of pH on phenol oxidase activity on decaying
927 *Sphagnum* mosses. *Eur. J. Soil Biol.* **54**, 41–47.

928 Tfaily M. M., Corbett J. E., Wilson R., Chanton J. P., Glaser P. H., Cawley K. M., Jaffé R. and
929 Cooper W. T. (2015) Utilization of PARAFAC-modeled excitation-emission matrix
930 (EEM) fluorescence spectroscopy to identify biogeochemical processing of dissolved
931 organic matter in a Northern peatland. *Photochem. Photobiol.* **91**, 684–695.

932 Tfaily M. M., Hamdan R., Corbett J. E., Chanton J. P., Glaser P. H. and Cooper W. T. (2013)
933 Investigating dissolved organic matter decomposition in northern peatlands using
934 complimentary analytical techniques. *Geochim. Cosmochim. Acta* **112**, 116–129.

935 Tfaily M. M., Hodgkins S., Podgorski D. C., Chanton J. P. and Cooper W. T. (2012) Comparison
936 of dialysis and solid-phase extraction for isolation and concentration of dissolved organic
937 matter prior to Fourier transform ion cyclotron resonance mass spectrometry. *Anal.*
938 *Bioanal. Chem.* **404**, 447–457.

939 Tfaily M. M., Podgorski D. C., Corbett J. E., Chanton J. P. and Cooper W. T. (2011) Influence of
940 acidification on the optical properties and molecular composition of dissolved organic
941 matter. *Anal. Chim. Acta* **706**, 261–267.

942 Thornton B. F., Wik M. and Crill P. M. (2015) Climate-forced changes in available energy and
943 methane bubbling from subarctic lakes. *Geophys. Res. Lett.* **42**, 1936–1942.

944 Tolonen K. and Turunen J. (1996) Accumulation rates of carbon in mires in Finland and
945 implications for climate change. *The Holocene* **6**, 171–178.

946 Turunen J., Tomppo E., Tolonen K. and Reinikainen A. (2002) Estimating carbon accumulation
947 rates of undrained mires in Finland – application to boreal and subarctic regions. *The*
948 *Holocene* **12**, 69–80.

949 Verhoeven J. T. A. and Liefveld W. M. (1997) The ecological significance of organochemical
950 compounds in *Sphagnum*. *Acta Bot. Neerlandica* **46**, 117–130.

951 Verhoeven J. T. A. and Toth E. (1995) Decomposition of *Carex* and *Sphagnum* litter in fens:
952 Effect of litter quality and inhibition by living tissue homogenates. *Soil Biol. Biochem.*
953 **27**, 271–275.

954 Wagner S., Riedel T., Niggemann J., Vähätalo A. V., Dittmar T. and Jaffé R. (2015) Linking the
955 molecular signature of heteroatomic dissolved organic matter to watershed characteristics
956 in world rivers. *Environ. Sci. Technol.* **49**, 13798–13806.

957 Walker S. A., Amon R. M. W. and Stedmon C. A. (2013) Variations in high-latitude riverine
958 fluorescent dissolved organic matter: A comparison of large Arctic rivers. *J. Geophys.*
959 *Res. Biogeosciences* **118**, 1689–1702.

960 Walter K. M., Smith L. C. and Stuart Chapin F. (2007) Methane bubbling from northern lakes:
961 present and future contributions to the global methane budget. *Philos. Trans. R. Soc.*
962 *Math. Phys. Eng. Sci.* **365**, 1657–1676.

963 Ward C. P. and Cory R. M. (2015) Chemical composition of dissolved organic matter draining
964 permafrost soils. *Geochim. Cosmochim. Acta* **167**, 63–79.

965 Weishaar J. L., Aiken G. R., Bergamaschi B. A., Fram M. S., Fujii R. and Mopper K. (2003)
966 Evaluation of specific ultraviolet absorbance as an indicator of the chemical composition
967 and reactivity of dissolved organic carbon. *Environ. Sci. Technol.* **37**, 4702–4708.

968 Williams C. J., Shingara E. A. and Yavitt J. B. (2000) Phenol oxidase activity in peatlands in
969 New York State: Response to summer drought and peat type. *Wetlands* **20**, 416–421.

970 Wingender J., Neu T. R. and Flemming H.-C. (1999) What are bacterial extracellular polymeric
971 substances? In *Microbial Extracellular Polymeric Substances* (eds. J. Wingender, T. R.
972 Neu, and H.-C. Flemming). Springer Berlin Heidelberg, Berlin. pp. 1–19. Available at:
973 http://dx.doi.org/10.1007/978-3-642-60147-7_1.

974 Xiang W., Wan X., Yan S., Wu Y. and Bao Z. (2013) Inhibitory effects of drought induced
975 acidification on phenol oxidase activities in *Sphagnum*-dominated peatland.
976 *Biogeochemistry* **116**, 293–301.

977 Yamashita Y., Panton A., Mahaffey C. and Jaffé R. (2011) Assessing the spatial and temporal
978 variability of dissolved organic matter in Liverpool Bay using excitation-emission matrix
979 fluorescence and parallel factor analysis. *Ocean Dyn.* **61**, 569–579.

980 Ye R., Jin Q., Bohannan B., Keller J. K., McAllister S. A. and Bridgham S. D. (2012) pH
981 controls over anaerobic carbon mineralization, the efficiency of methane production, and
982 methanogenic pathways in peatlands across an ombrotrophic–minerotrophic gradient.
983 *Soil Biol. Biochem.* **54**, 36–47.

984 Zepp R. G., Sheldon W. M. and Moran M. A. (2004) Dissolved organic fluorophores in
985 southeastern US coastal waters: correction method for eliminating Rayleigh and Raman
986 scattering peaks in excitation-emission matrices. *Mar. Chem.* **89**, 15–36.

987 Zsolnay A., Baigar E., Jimenez M., Steinweg B. and Saccomandi F. (1999) Differentiating with
988 fluorescence spectroscopy the sources of dissolved organic matter in soils subjected to
989 drying. *Chemosphere* **38**, 45–50.

990

991 **FIGURE CAPTIONS**

992 **Fig. 1.** Differences in elemental composition between six bog and six rich fen samples, as
993 revealed by FT-ICR MS. Compounds are plotted according to (a) elemental composition
994 via a van Krevelen plot of O/C and H/C, with compound classes defined in Table 2
995 identified by boxes, and (b) molecular size, specifically C number and MW. Colors
996 indicate the difference in each compound's average relative abundance between bogs and
997 rich fens, calculated as described in "2.7.1. Elemental composition." Green or purple
998 points indicate compounds more abundant in bogs or rich fens, respectively, and the color
999 saturation indicates the absolute value of the difference.

1000 **Fig. 2.** FT-ICR MS results, presented as abundance-weighted average MW; O/C, H/C, N/C, and
1001 S/C; and relative abundances of FT-ICR MS compound classes (defined in Table 2) in
1002 each sample. Abbreviations of compound classes are as follows: AS.carb = aminosugar +
1003 carbohydrate, UH = unsaturated hydrocarbon, CA = condensed aromatic. Due to the
1004 presence of formulas that did not fit in any of the compound classes, their abundances do
1005 not add to exactly 100%. Different individual sites are denoted by color, and
1006 characteristics of the samples are given in Table 1. The % lipid-like compounds in
1007 sample E.1.26 is indicated by a number because it was much higher than that of the other
1008 samples.

1009 **Fig. 3.** Optical properties for each sample, presented as SUVA, BIX, HIX, Em_{max}, and F_{max}/A_{340}
1010 (defined in "2.7.2. Bulk optical properties"); and relative abundances of the five
1011 PARAFAC components (defined in "2.7.3. PARAFAC model"). Different individual
1012 sites are denoted by color, and characteristics of the samples are given in Table 1.

1013 **Fig. 4.** Principal components analyses (PCA) of (a) FT-ICR MS average molecular
1014 characteristics and bulk optical properties, and (b) FT-ICR MS compound class and

1015 PARAFAC component relative abundances. Scores for each sample are shown as points,
1016 and variable loadings for each PC are shown as labeled arrows and summarized in "3.4.
1017 Correlation of optical properties with FT-ICR MS."

1018 **Fig. 5.** Strong negative correlation between the PARAFAC components C1 and C3.

1019

1020

1021

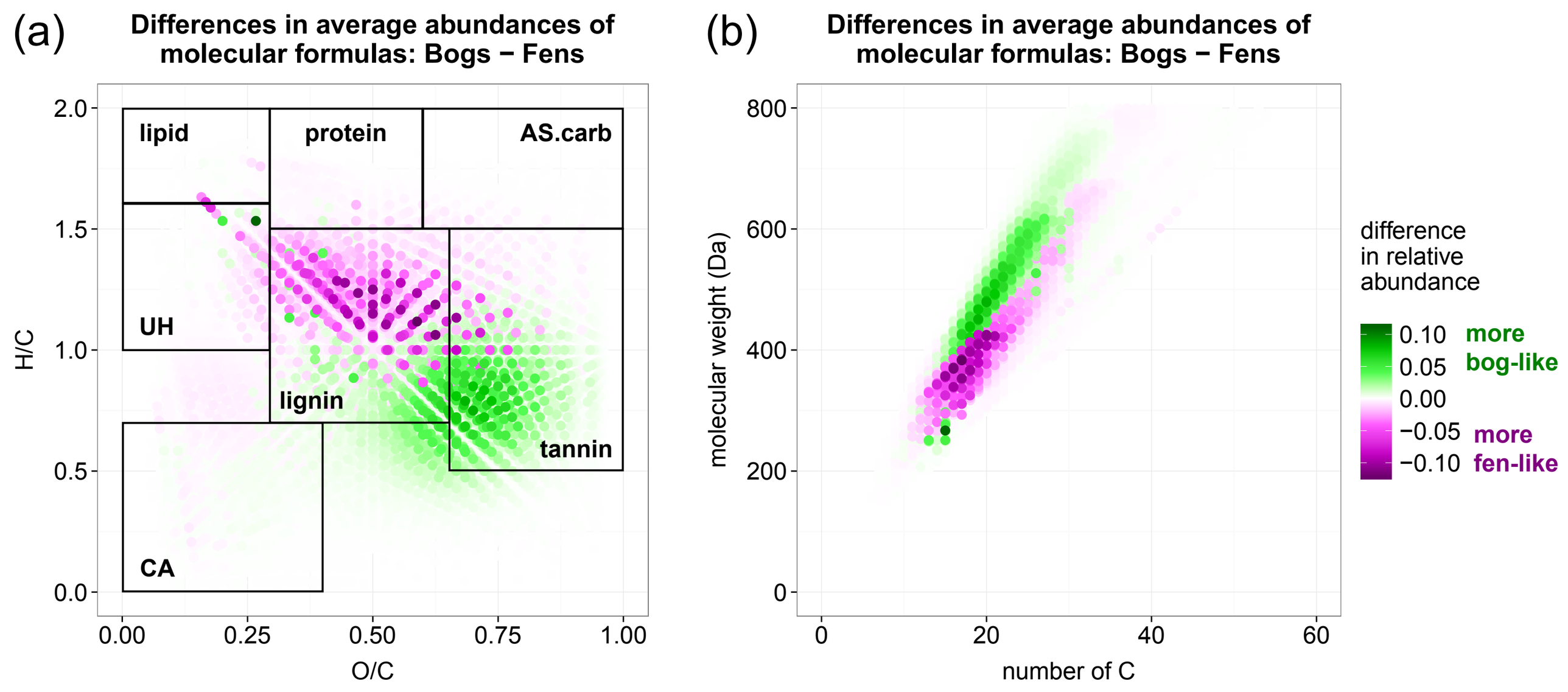
(a)
Differences in average abundances of molecular formulas: Bogs − Fens
lipid
protein
AS.carb
UH
lignin
tannin
CA
H/C
O/C
2.0
1.5
1.0
0.5
0.0
0.00
0.25
0.50
0.75
1.00
(b)
Differences in average abundances of molecular formulas: Bogs − Fens
molecular weight (Da)
number of C
800
600
400
200
0
0
20
40
60
difference in relative abundance
0.10
0.05
0.00
−0.05
−0.10
more bog-like
more fen-like

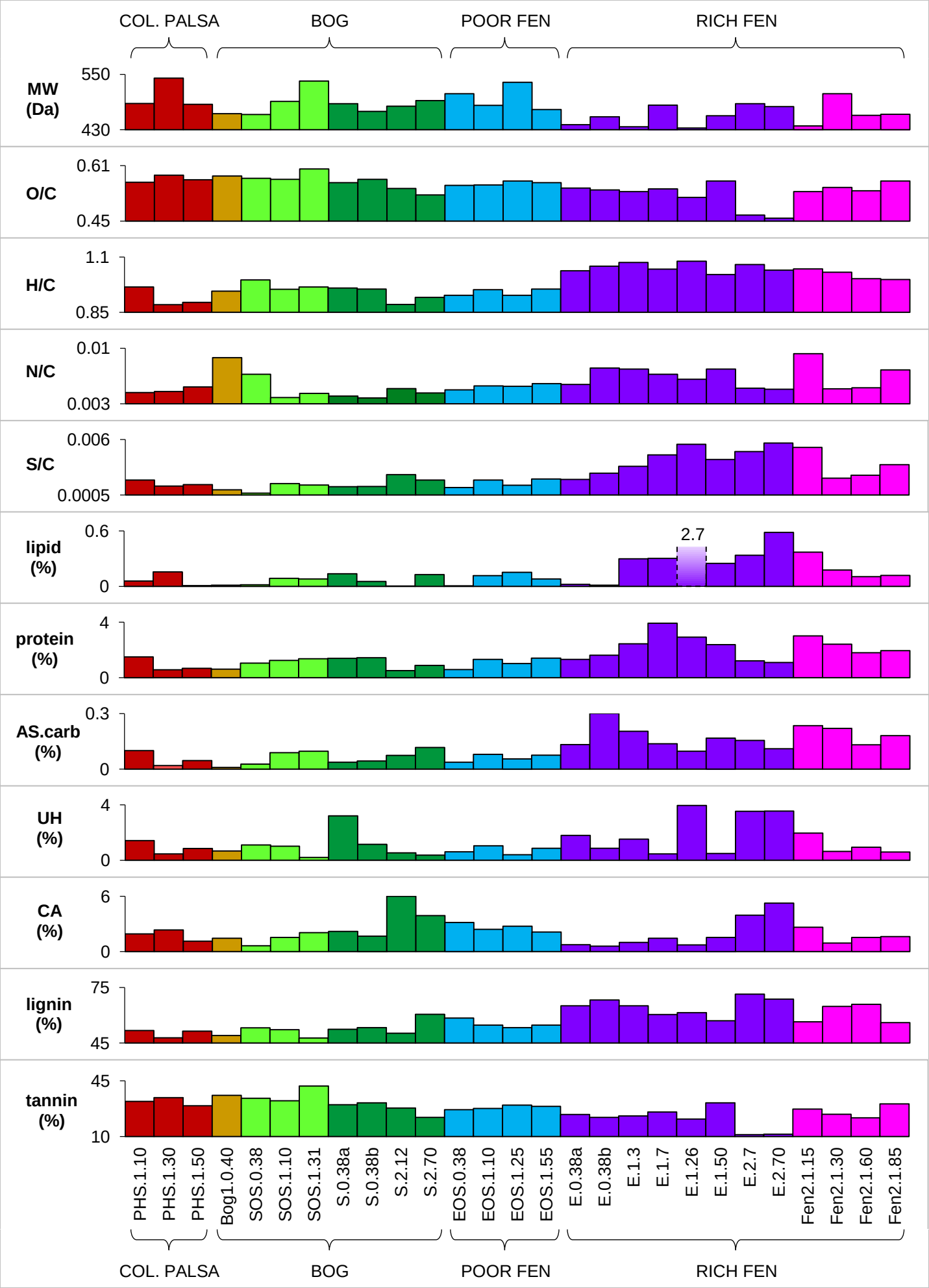
COL. PALSA
BOG
POOR FEN
RICH FEN
MW (Da)
550
430
O/C
0.61
0.45
H/C
1.1
0.85
N/C
0.01
0.003
S/C
0.006
0.0005
lipid (%)
0.6
0
2.7
protein (%)
4
0
AS.carb (%)
0.3
0
UH (%)
4
0
CA (%)
6
0
lignin (%)
75
45
tannin (%)
45
10
PHS.1.10
PHS.1.30
PHS.1.50
Bog1.0.40
SOS.0.38
SOS.1.10
SOS.1.31
S.0.38a
S.0.38b
S.2.12
S.2.70
EOS.0.38
EOS.1.10
EOS.1.25
EOS.1.55
E.0.38a
E.0.38b
E.1.3
E.1.7
E.1.26
E.1.50
E.2.7
E.2.70
Fen2.1.15
Fen2.1.30
Fen2.1.60
Fen2.1.85
COL. PALSA
BOG
POOR FEN
RICH FEN

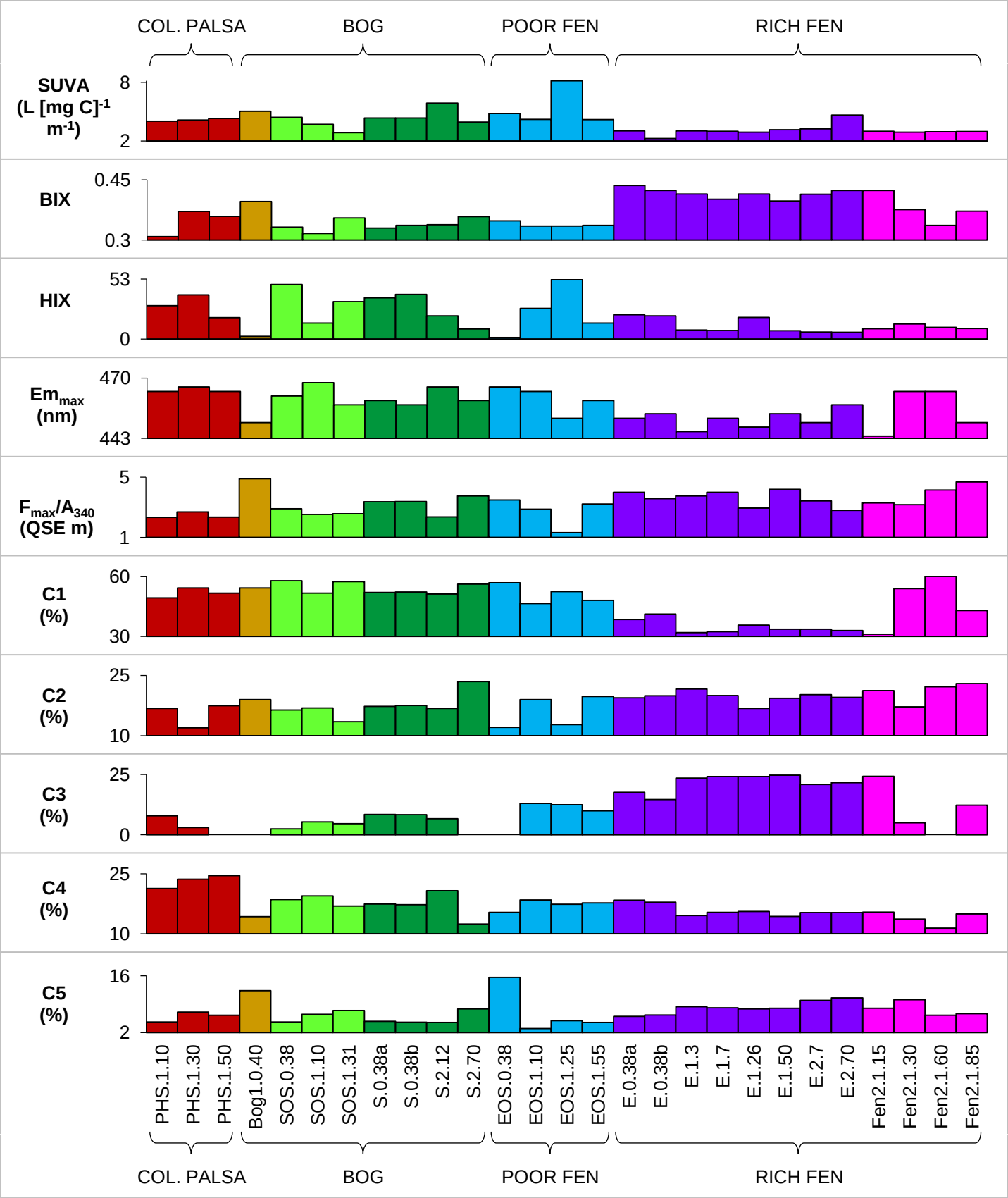
COL. PALSA
BOG
POOR FEN
RICH FEN
SUVA (L [mg C]-1 m-1)
8
2
BIX
0.45
0.3
HIX
53
0
Emmax (nm)
470
443
Fmax/A340 (QSE m)
5
1
C1 (%)
60
30
C2 (%)
25
10
C3 (%)
25
0
C4 (%)
25
10
C5 (%)
16
2
PHS.1.10
PHS.1.30
PHS.1.50
Bog1.0.40
SOS.0.38
SOS.1.10
SOS.1.31
S.0.38a
S.0.38b
S.2.12
S.2.70
EOS.0.38
EOS.1.10
EOS.1.25
EOS.1.55
E.0.38a
E.0.38b
E.1.3
E.1.7
E.1.26
E.1.50
E.2.7
E.2.70
Fen2.1.15
Fen2.1.30
Fen2.1.60
Fen2.1.85
COL. PALSA
BOG
POOR FEN
RICH FEN

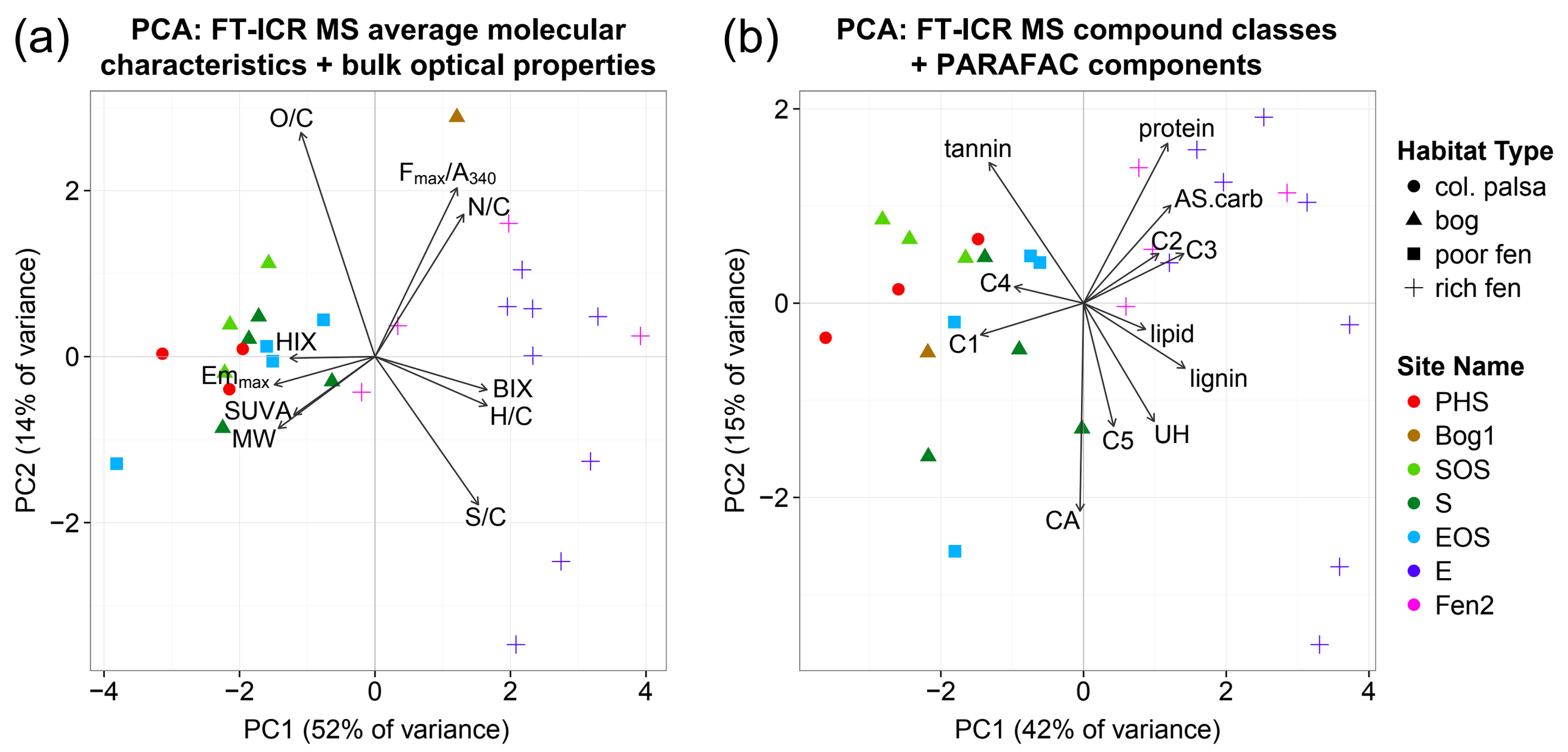
(a)
PCA: FT-ICR MS average molecular characteristics + bulk optical properties
O/C
F_{max}/A_{340}
N/C
HIX
Em_{max}
SUVA
MW
BIX
H/C
S/C
PC2 (14% of variance)
PC1 (52% of variance)
(b)
PCA: FT-ICR MS compound classes + PARAFAC components
tannin
protein
AS.carb
C2
C3
C4
C1
lipid
lignin
C5
UH
CA
PC2 (15% of variance)
PC1 (42% of variance)
Habitat Type
col. palsa
bog
poor fen
rich fen
Site Name
PHS
Bog1
SOS
S
EOS
E
Fen2

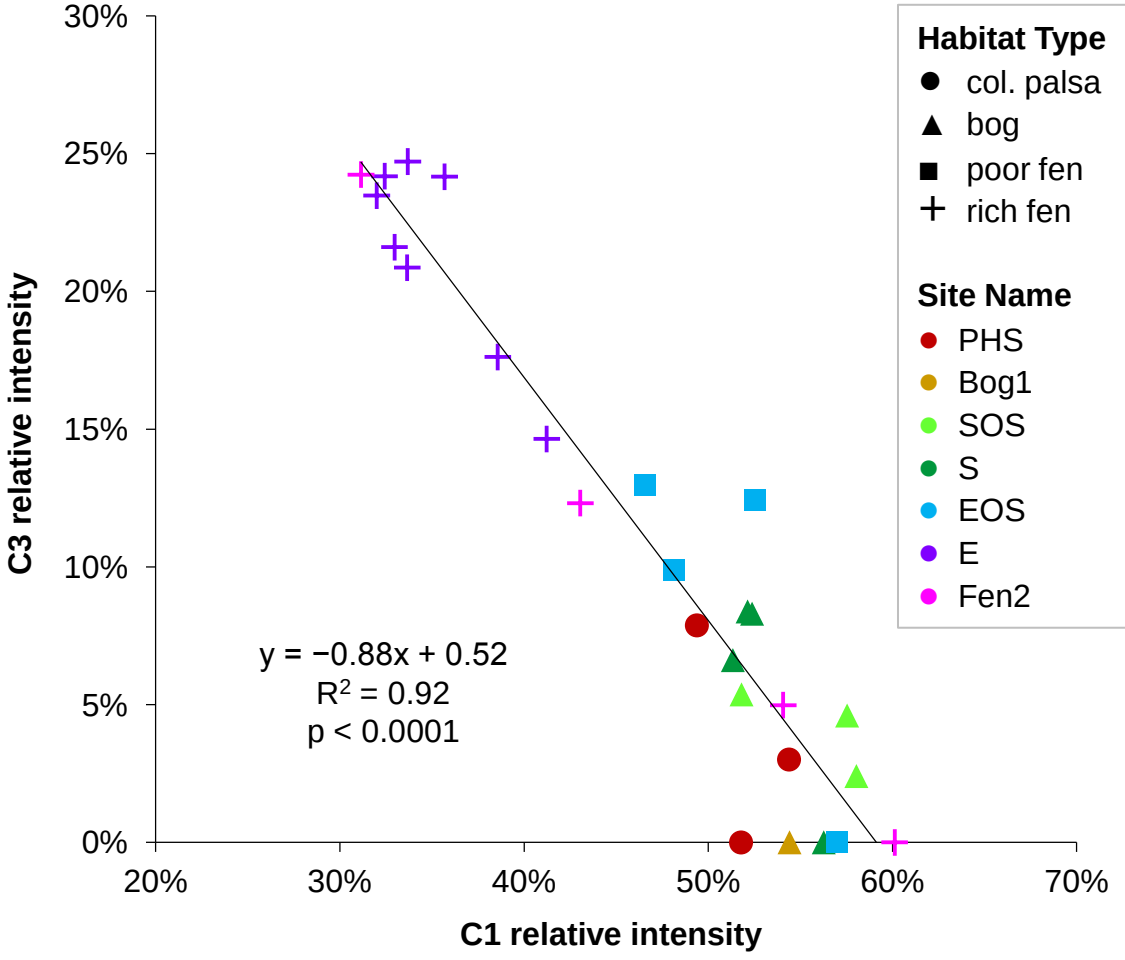
30%
25%
20%
15%
10%
5%
0%
20%
30%
40%
50%
60%
70%
C3 relative intensity
C1 relative intensity
y = −0.88x + 0.52
R2 = 0.92
p < 0.0001
Habitat Type
col. palsa
bog
poor fen
rich fen
Site Name
PHS
Bog1
SOS
S
EOS
E
Fen2

1022 Table 1. Characteristics of the samples gathered for this study. Horizontal lines separate samples
1023 gathered from the same site at the same time. For the samples from sites S and E gathered on
1024 Sept. 1, 2010, the labels "a" and "b" correspond to replicate samples from the same depth.

Sample Name	Habitat Type	Site	Depth (cm)	Sampling Date	pH	DOC (mM)
PHS.1.10	col. palsa	PHS	10	13 Jun 2011	4.0	4.60
PHS.1.30	col. palsa	PHS	30	13 Jun 2011	4.1	5.35
PHS.1.50	col. palsa	PHS	50	13 Jun 2011	4.3	8.62
Bog1.0.40	bog	Bog1	40	31 Aug 2010	3.6	10.58
SOS.0.38	bog	SOS	37.5	31 Aug 2010	3.7	4.00
SOS.1.10	bog	SOS	10	13 Jun 2011	4.0	6.10
SOS.1.31	bog	SOS	31	13 Jun 2011	4.0	5.13
S.0.38a	bog	S	37.5	1 Sep 2010	3.9	3.77
S.0.38b	bog	S	37.5	1 Sep 2010	3.9	3.72
S.2.12	bog	S	12	21 Aug 2012	4.2	5.08
S.2.70	bog	S	70	21 Aug 2012	5.0	6.42
EOS.0.38	poor fen	EOS	37.5	31 Aug 2010	3.7	6.35
EOS.1.10	poor fen	EOS	10	13 Jun 2011	4.9	2.55
EOS.1.25	poor fen	EOS	25	13 Jun 2011	4.6	3.46
EOS.1.55	poor fen	EOS	55	13 Jun 2011	4.9	3.17
E.0.38a	rich fen	E	37.5	1 Sep 2010	5.4	0.72
E.0.38b	rich fen	E	37.5	1 Sep 2010	5.5	0.90
E.1.3	rich fen	E	2.5	15 Jun 2011	6.0	0.69
E.1.7	rich fen	E	6.5	15 Jun 2011	6.0	0.74
E.1.26	rich fen	E	25.5	15 Jun 2011	6.0	0.78
E.1.50	rich fen	E	50	15 Jun 2011	5.7	0.80
E.2.7	rich fen	E	7	21 Aug 2012	5.9	0.61
E.2.70	rich fen	E	70	21 Aug 2012	6.2	0.61
Fen2.1.15	rich fen	Fen2	15	14 Jun 2011	5.8	0.53
Fen2.1.30	rich fen	Fen2	30	14 Jun 2011	5.5	1.19
Fen2.1.60	rich fen	Fen2	60	14 Jun 2011	5.4	2.42
Fen2.1.85	rich fen	Fen2	85	14 Jun 2011	5.7	1.09

1025
1026

1027

1028 Table 2. Characteristics of compound classes used to categorize FT-ICR MS molecular formulas.

Compound Class	Abbreviation	O/C range	H/C range
lipid-like	lipid	0–0.29	1.6–2
protein-like	protein	0.29–0.6	1.5–2
aminosugar and carbohydrate-like	AS.carb	0.6–1	1.5–2
unsaturated hydrocarbons	UH	0–0.29	1–1.6
condensed aromatics	CA	0–0.4	0–0.7
lignin-like	lignin	0.29–0.65	0.7–1.5
tannin-like	tannin	0.65–1	0.5–1.5

1029
1030
1031
1032

Table 3. P-values from one-way ANOVAs comparing each variable across habitat types and sites, and paired t-tests comparing each variable between the shallowest and deepest sample in each depth profile that had >1 depth. "—" = not significant, with cutoff at p = 0.05. Abbreviations: DOC = dissolved organic carbon; MW = molecular weight; O/C, H/C, N/C, and S/C = elemental ratios. Compound classes (putative; see Table 2): AS.carb = aminosugar- and carbohydrate-like; UH = unsaturated hydrocarbon; CA = condensed aromatic. Optical properties (see "2.7.2. Bulk optical properties"): SUVA = specific UV absorbance; BIX = biological index; HIX = humification index; Em_{max} = emission wavelength of peak C maximum; F_{max}/A_{340} = ratio of peak C fluorescence intensity to absorbance at 340 nm. PARAFAC components (see "2.7.3. PARAFAC model" and Table A.1): C1 = plant-derived humic-like; C2 and C3 = microbially-derived humic-like; C4 = high molecular weight aromatic humic-like or terrestrial reduced quinone-like; C5 = protein-like.

	one-way ANOVA		paired t-test		
	Habitat Type	Site	Depth (all sites)	Depth (rich fens only)	Depth (sites with *Sphagnum*)
General pore water chemistry:					
pH	1e–9	3e–8	—	—	—
DOC	2e–6	1e–7	—	—	—
Elemental composition (FT-ICR MS):					
MW	0.02	—	—	—	—
O/C	0.02	0.03	—	—	—
H/C	6e–8	2e–7	—	0.04	—
N/C	—	0.01	—	—	—
S/C	7e–5	0.001	—	—	—
lipid	—	—	—	—	—
protein	0.002	0.02	—	—	—
AS.carb	6e–5	0.0008	—	0.01	—
UH	—	—	0.02	—	—
lignin	1e–5	0.0001	—	—	—
tannin	0.005	0.004	—	—	—
CA	—	—	—	—	—
Optical properties:					
SUVA	0.002	0.01	—	—	—
BIX	8e–5	1e–5	—	—	—
HIX	—	—	—	—	—
Em_{max}	0.009	0.01	—	0.008	—
F_{max}/A_{340}	0.03	0.008	—	—	—
C1	0.0003	0.0001	0.05	—	0.03
C2	0.02	0.04	—	—	—
C3	0.0006	0.0002	—	—	—
C4	6e–5	0.0002	—	—	—
C5	—	—	—	—	0.04